MICROWAVE REMOTE SENSING THEORY

Microwave remote sensing of the earth has advantages over other remote sensing techniques, in that microwaves can penetrate clouds and also provide day and night coverage. Recent advances in microwave remote sensing measurements include synthetic aperture radar (SAR), imaging radar, interferometric SAR, spotlight SAR, circular SAR for active remote sensing, polarimetric radiometry, and SAR for passive remote sensing. The emphasis of this article is on how microwaves interact with geophysical terrain such as snow, ice, soils, forests, vegetation, rocky terrain, ocean, and sea surface. The scattering effects of such media contribute to microwave measurements. The scattering effects can be divided into surface scattering and volume scattering. This article describes the analytic and numerical approaches for treating such effects. Microwave remote sensing is a broad subject. We refer the reader to other articles in this encyclopedia for measurement techniques of antennas, radars, and radiometers, signal and image processing techniques, molecular theory of microwave radiation of gases, etc.

The scattering effects of geophysical terrain can be characterized by random rough surface scattering and volume scattering from inhomogenities of the medium. In rough surface scattering, the rough surface has many peaks and valleys and the height profile can be described by random processes (1–3). In volume scattering, there are many particles that interact with microwaves. The positions of these particles are random. Such volume scattering effects are described by random distribution of wave scattering (2,4–6). This article studies the wave scattering by random rough surfaces and random discrete scatterers and their applications to microwave interaction with geophysical media in the context of microwave remote sensing. At microwave frequency, the size of the scatterers and the rough surface heights in a geophysical terrain are comparable to microwave wavelengths. Thus, the use of the wave approach based on solutions of Maxwell's equations is essential.

First, we review the basic principles of microwave interaction in active remote sensing and passive remote sensing. Next, we describe vector radiative transfer theory (2,7), which treats volume scattering and the small perturbation method for treating rough surface scattering. With the advent of modern computers and the development of computation methods, recent research in scattering problems emphasizes Monte Carlo simulations of solutions of Maxwell's equations. These consist in generating samples or realizations of rough surface and random discrete scatterers and then using numerical methods to solve Maxwell's equations for such boundary value problems. In the final section, we describe the results of such approaches.

BASICS OF MICROWAVE REMOTE SENSING

Active Remote Sensing

We first consider the radar equation for scattering by a conglomeration of scatterers (Fig. 1). Consider a volume V containing a random distribution of particles. The volume is illuminated by a transmitter in the direction of $\hat{\boldsymbol{k}}_i$ where $\hat{\boldsymbol{k}}_i$ is the unit vector in the direction of incident wave propagation. The scattered wave in the direction $\hat{\boldsymbol{k}}_s$ is received by the receiver. Consider a differential volume dV containing $N_0 = n_0 dV$ num-

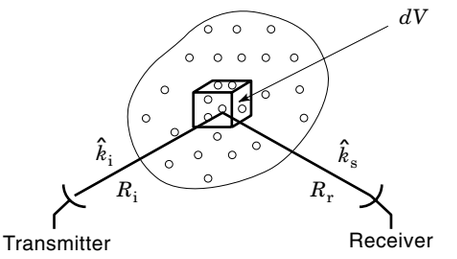

Figure 1. Scattering by a conglomeration of scatterers. The scattering geometry for remote sensing, showing both the transmitter and the receiver.

ber of particles, where n_0 is the number of particles per unit volume. The Poynting vector $\boldsymbol{S}_\mathrm{i}$ incident on dV is

$$S_\mathrm{i} = \frac{G_\mathrm{t}(\hat{\boldsymbol{k}}_\mathrm{i})P_\mathrm{t}}{4\pi R_\mathrm{i}^2} \tag{1}$$

where P_t is the power transmitted by the transmitter, $G_\mathrm{t}(\hat{\boldsymbol{k}}_\mathrm{i})$ is the gain of the transmitter in the direction $\hat{\boldsymbol{k}}_\mathrm{i}$, and R_i is the distance between the transmitter and dV.

Let $\sigma_\mathrm{d}^{(N_0)}(\hat{\boldsymbol{k}}_\mathrm{s}, \hat{\boldsymbol{k}}_\mathrm{i})$ denote the differential scattering cross section of the N_0 particles in dV. The physical size of dV is chosen so that

$$\sigma_\mathrm{d}^{(N_0)}(\hat{\boldsymbol{k}}_\mathrm{s}, \hat{\boldsymbol{k}}_\mathrm{i}) = p(\hat{\boldsymbol{k}}_\mathrm{s}, \hat{\boldsymbol{k}}_\mathrm{i})\, dV \tag{2}$$

which means $\sigma_\mathrm{d}^{(N_0)}$ is proportional to dV and $p(\hat{\boldsymbol{k}}_\mathrm{s}, \hat{\boldsymbol{k}}_\mathrm{i})$ is the differential cross section per unit volume. The measured power at the receiver due to dV is

$$dP = A_\mathrm{r}(\hat{\boldsymbol{k}}_\mathrm{s}) \frac{\sigma_\mathrm{d}^{(N_0)}(\hat{\boldsymbol{k}}_\mathrm{s}, \hat{\boldsymbol{k}}_\mathrm{i})}{R_\mathrm{r}^2} S_\mathrm{i} \tag{3}$$

where R_r is the distance between dV and the receiver, and $A_\mathrm{r}(\hat{\boldsymbol{k}}_\mathrm{s})$ is the effective receiver area of the receiving antenna.

$$A_\mathrm{r}(\hat{\boldsymbol{k}}_\mathrm{s}) = \frac{G_\mathrm{r}(\hat{\boldsymbol{k}}_\mathrm{s})\lambda^2}{4\pi} \tag{4}$$

where $G_\mathrm{r}(\hat{\boldsymbol{k}}_\mathrm{s})$ is the gain of the receiver in direction $\hat{\boldsymbol{k}}_\mathrm{s}$. Putting together Eqs. (1) to (4) and integrating over volume dV gives the receiver power P_r as

$$\frac{P_\mathrm{r}}{P_\mathrm{t}} = \int dV \frac{\lambda^2}{(4\pi)^2} \frac{G_\mathrm{t}(\hat{\boldsymbol{k}}_\mathrm{i})G_\mathrm{r}(\hat{\boldsymbol{k}}_\mathrm{s})}{R_\mathrm{i}^2 R_\mathrm{r}^2}\, p(\hat{\boldsymbol{k}}_\mathrm{s}, \hat{\boldsymbol{k}}_\mathrm{i}) \tag{5}$$

Equation (5) is the radar equation for bistatic scattering of a volume of scatterers. For monostatic radar, the scattered direction is opposite to that of the incident direction $\hat{\boldsymbol{k}}_\mathrm{s} = -\hat{\boldsymbol{k}}_\mathrm{i}$ and we have for $R_\mathrm{r} = R_\mathrm{i} = R$

$$\frac{P_\mathrm{r}}{P_\mathrm{t}} = \int dV \frac{\lambda^2}{(4\pi)^2} \frac{[G_\mathrm{t}(\hat{\boldsymbol{k}}_\mathrm{i})]^2}{R^4}\, p(-\hat{\boldsymbol{k}}_\mathrm{i}, \hat{\boldsymbol{k}}_\mathrm{i}) \tag{6}$$

Equations (5) and (6) are the radar equation for a conglomeration of scatters.

In independent scattering, we assume that the scattering cross sections of particles are additive. For the case that the particles scatter independently, and assuming that the N_0 particles are identical,

$$\sigma_\mathrm{d}^{(N_0)}(\hat{\boldsymbol{k}}_\mathrm{s}, \hat{\boldsymbol{k}}_\mathrm{i}) = N_0 \sigma_\mathrm{d}(\hat{\boldsymbol{k}}_\mathrm{s}, \hat{\boldsymbol{k}}_\mathrm{i}) \tag{7}$$

where $\sigma_\mathrm{d}(\hat{\boldsymbol{k}}_\mathrm{s}, \hat{\boldsymbol{k}}_\mathrm{i})$ is the differential cross section of one particle. From Eqs. (2) and (7) and from $N_0 = n_0 dV$, we have

$$p(\hat{\boldsymbol{k}}_\mathrm{s}, \hat{\boldsymbol{k}}_\mathrm{i}) = n_0 \sigma_\mathrm{d}(\hat{\boldsymbol{k}}_\mathrm{s}, \hat{\boldsymbol{k}}_\mathrm{i}) \tag{8}$$

For scattering by a small sphere of relative permittivity ϵ_r and radius a, the differential cross section is

$$\sigma_d = k^4 a^6 \left| \frac{\epsilon_\mathrm{r} - 1}{\epsilon_\mathrm{r} + 2} \right|^2$$

Let $f = (4\pi/3)a^3 n_0$ be the fractional volume occupied by the particles, then

$$N_0 = \frac{Vf}{(4\pi/3)a^3}$$

and

$$\sigma_\mathrm{d}^{(N_0)} = N_0 \sigma_\mathrm{d} = \frac{3}{4\pi}(Vfk)(ka)^3 \left| \frac{\epsilon_\mathrm{r} - 1}{\epsilon_\mathrm{r} + 2} \right|^2$$

Similarly, we define

$$\kappa_\mathrm{s} = \text{scattering cross section per unit volume} \tag{9}$$

$$\kappa_\mathrm{a} = \text{absorption cross section per unit volume} \tag{10}$$

$$\kappa_\mathrm{e} = \text{extinction cross section per unit volume} \tag{11}$$

Then

$$\kappa_\mathrm{s} = \int_{4\pi} d\Omega_\mathrm{s} p(\hat{\boldsymbol{k}}_\mathrm{s}, \hat{\boldsymbol{k}}_\mathrm{i}) \tag{12}$$

where integration is over 4π scattered directions. Using independent scattering, we have

$$\kappa_\mathrm{s} = n_0 \int_{4\pi} d\Omega_\mathrm{s} \sigma_\mathrm{d}(\hat{\boldsymbol{k}}_\mathrm{s}, \hat{\boldsymbol{k}}_\mathrm{i}) = n_0 \sigma_\mathrm{s} \tag{13}$$

$$\kappa_\mathrm{a} = n_0 \sigma_\mathrm{a} \tag{14}$$

For a spherical particle with radius a and relative permittivity ϵ_r,

$$\sigma_a = v_0 k \epsilon_\mathrm{r}'' \left| \frac{3}{\epsilon_\mathrm{r} + 2} \right|^2$$

where ϵ_r'' is the imaginary part of ϵ_r. The extinction is the sum of scattering and absorption.

$$\kappa_\mathrm{e} = \kappa_\mathrm{s} + \kappa_\mathrm{a} = n_0(\sigma_\mathrm{s} + \sigma_\mathrm{a}) \tag{15}$$

The parameters κ_s, κ_a, and κ_e are also known respectively as scattering coefficient, absorption coefficient, and extinction coefficient.

Consider intensity I that has dimension of power per unit area incident on a slab of thickness Δz and cross-section area A. Then the power extinguished by the scatterers is $\Delta P = -$(intensity) (extinction cross section per unit volume) (volume)

$$\begin{aligned} \Delta P &= -I\kappa_\mathrm{e} A\, \Delta z \\ &= \Delta I A \end{aligned}$$

Hence $\Delta I/\Delta z = -\kappa_\mathrm{e} I$ giving the solution $I = I_0 e^{-\kappa_\mathrm{e} s}$, where s is the distance traveled by the wave. Thus κ_e represents attenu-

ation per unit distance due to absorption and scattering. If attenuation is inhomogeneous, we have an attenuation factor of

$$\gamma = \int \kappa_e \, ds$$

where ds is the differential distance the wave travels. Attenuation can be included in the radar equation so that

$$\frac{P_r}{P_t} = \int dV \frac{\lambda^2}{(4\pi)^2} \frac{G_t(\hat{\boldsymbol{k}}_i) G_r(\hat{\boldsymbol{k}}_s)}{R_i^2 R_r^2} p(\hat{\boldsymbol{k}}_s, \hat{\boldsymbol{k}}_i) \exp(-\gamma_i - \gamma_r) \quad (16)$$

where

$$\gamma_i = \int \kappa_e \, ds \quad (17)$$

is the attenuation from transmitting antenna to dV and

$$\gamma_r = \int \kappa_e \, ds \quad (18)$$

is the attenuation from dV to receiving antenna.

Particle Size Distribution. In many cases, the particles obey a size distribution $n(a)$ so that the number of particles per unit volume with size between a and $a + da$ is $n(a)da$. Thus

$$n_0 = \int_0^\infty n(a) \, da \quad (19)$$

Within the approximation of independent scattering,

$$\kappa_s = \int_0^\infty n(a) \sigma_s(a) \, da \quad (20)$$

where $\sigma_s(a)$ is the scattering cross section for a particle of radius a. Also

$$\kappa_a = \int_0^\infty n(a) \sigma_a(a) \, da \quad (21)$$

$$p(\hat{\boldsymbol{k}}_s, \hat{\boldsymbol{k}}_i) = \int_0^\infty n(a) \sigma_d(\hat{\boldsymbol{k}}_s, \hat{\boldsymbol{k}}_i; a) \, da \quad (22)$$

For Rayleigh scattering by spheres

$$p(\hat{\boldsymbol{k}}_s, \hat{\boldsymbol{k}}_i) = k^4 \left| \frac{\epsilon_r - 1}{\epsilon_r + 2} \right|^2 |\hat{\boldsymbol{k}}_s \times (\hat{\boldsymbol{k}}_s \times \hat{\boldsymbol{e}}_i)|^2 \int_0^\infty n(a) a^6 \, da \quad (23)$$

$$\kappa_s = \frac{8\pi}{3} k^4 \left| \frac{\epsilon_r - 1}{\epsilon_r - 2} \right|^2 \int_0^\infty n(a) a^6 \, da \quad (24)$$

$$\kappa_a = \frac{4\pi}{3} k \frac{\epsilon_p''}{\epsilon} \left| \frac{3\epsilon}{\epsilon_p + 2\epsilon} \right|^2 \int_0^\infty n(a) a^3 \, da \quad (25)$$

A typical example is rainfall where the raindrops are described by a size distribution known as the Marshall–Palmer size distribution of exponential dependence $n(a) = n_D e^{-\alpha a}$, with $n_D = 8 \times 10^6$ m^{-4} and $\alpha = (8200/P^{0.21})$ m^{-1}, and P is the precipitation rate in millimeters per hour.

Bistatic Scattering Coefficients

For active remote sensing of the surface of the earth, the radar equation is

$$\frac{P_r}{P_t} = \frac{G_t}{4\pi r_t^2} \exp(-\gamma_t) \frac{\sigma_A}{4\pi r^2} \frac{G_r \lambda^2}{4\pi} \exp(-\gamma_r) \quad (26)$$

Thus, in terms of scattering characteristics of the surface of the earth, the quantity of interest to be calculated is σ_A. For the case of terrain and sea returns, the cross section is often normalized with respect to the area A that is illuminated by radar. The bistatic scattering coefficient is defined as

$$\gamma_{\beta\alpha}(\theta_s, \varphi_s; \theta_i, \varphi_i) = \lim_{r \to \infty} \frac{4\pi r^2 |E_\beta^s|^2}{|E_\alpha^i|^2 A \cos\theta_i} \quad (27)$$

where E_β^s denotes the β polarization component of the scattered electric field and E_α^i is the incident field with α polarization. Given the bistatic scattering coefficient $\gamma_{\beta\alpha}$, then the scattering cross section is $\sigma_A = A\gamma_{\beta\alpha}$.

Notice that $A \cos\theta_i$ is the illuminated area projected onto the plane normal to the incident direction. From Fig. 2, the incident and scattered directions $\hat{\boldsymbol{k}}_i$ and $\hat{\boldsymbol{k}}_s$ can be written as follows:

$$\hat{\boldsymbol{k}}_i = \sin\theta_i \cos\varphi_i \hat{\boldsymbol{x}} + \sin\theta_i \sin\varphi_i \hat{\boldsymbol{y}} - \cos\theta_i \hat{\boldsymbol{z}} \quad (28a)$$

$$\hat{\boldsymbol{k}}_s = \sin\theta_s \cos\varphi_s \hat{\boldsymbol{x}} + \sin\theta_s \sin\varphi_s \hat{\boldsymbol{y}} + \cos\theta_s \hat{\boldsymbol{z}} \quad (28b)$$

In the backscattering direction $\theta_s = \theta_i$ and $\varphi_s = \pi + \varphi_i$, the monostatic (backscattering) coefficient is defined as,

$$\sigma_{\beta\alpha}(\theta_i, \varphi_i) = \cos\theta_i \gamma_{\beta\alpha}(\theta_s = \theta_i, \varphi_s = \pi + \varphi_i; \theta_i, \varphi_i) \quad (29)$$

Stokes Parameters

Consider a time harmonic elliptically polarized radiation field with time dependence $\exp(-i\omega t)$ propagating in the $\hat{\boldsymbol{k}}$ direction with complex electric field given by

$$\overline{E} = E_v \hat{\boldsymbol{v}} + E_h \hat{\boldsymbol{h}} \quad (30)$$

Where $\hat{\boldsymbol{v}}$ and $\hat{\boldsymbol{h}}$ denote the two orthogonal polarizations with $\hat{\boldsymbol{k}}$, $\hat{\boldsymbol{v}}$, and $\hat{\boldsymbol{h}}$ following the right-hand rule. Thus

$$\epsilon_v(t) = \mathrm{Re}(E_v e^{-i\omega t}) \quad (31a)$$

$$\epsilon_h(t) = \mathrm{Re}(E_h e^{-i\omega t}) \quad (31b)$$

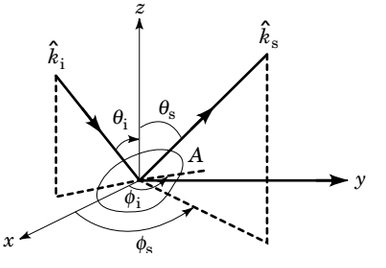

Figure 2. Incident and scattered directions in calculating bistatic scattering coefficients. The incident wave in the direction of $\hat{\boldsymbol{k}}_i$ impinges on the target and is scattered in the direction of $\hat{\boldsymbol{k}}_s$.

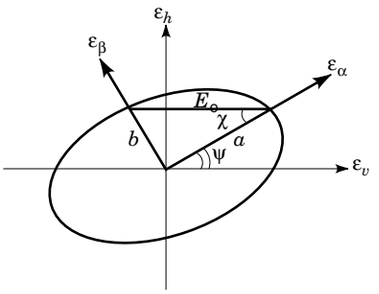

Figure 3. Elliptical polarization ellipse with major and minor axes. The trace of the tip of the E vector at a given point in space as a function of time for an elliptically polarized wave.

Let

$$E_v = E_{v0}e^{i\delta_v} \tag{32a}$$

$$E_h = E_{h0}e^{i\delta_h} \tag{32b}$$

There are three independent parameters that describe the elliptical polarization. We shall describe three ways of describing polarization.

(A) The three parameters are E_{v0}, E_{h0}, and phase difference $\delta = \delta_v - \delta_h$.

(B) For a general elliptically polarized wave, the ellipse may not be upright. It is tilted at an angle ψ with respect to v and h (Fig. 3). The second description is using E_0, χ, and ψ. Where χ is the ellipticity angle and ψ is the orientation angle.

Let a and b be the lengths of semimajor axis and semiminor axis, respectively, and LH and RH stand for left hand and right hand polarized respectively. Let χ be defined so that

$$\tan\chi = b/a \quad \text{if LH} \tag{33a}$$

$$\tan\chi = -b/a \quad \text{if RH} \tag{33b}$$

Also,

$$\sqrt{a^2 + b^2} = E_0 \tag{34}$$

Then for LH

$$b = E_0 \sin\chi \tag{35a}$$

$$a = E_0 \cos\chi \tag{35b}$$

and for RH

$$b = -E_0 \sin\chi \tag{36a}$$

$$a = E_0 \cos\chi \tag{36b}$$

By performing a rotation of axis, it follows that

$$E_v = iE_0 \cos\chi \cos\psi - E_0 \sin\chi \sin\psi \tag{37a}$$

$$E_h = iE_0 \cos\chi \sin\psi + E_0 \sin\chi \cos\psi \tag{37b}$$

Equations (37a) and (37b) give the relation between polarization descriptions of (A) and (B).

(C) The third polarization description is that of Stokes parameters. There are four Stokes parameters. They are

$$I_v = \frac{|E_v|^2}{\eta} \tag{38a}$$

$$I_h = \frac{|E_h|^2}{\eta} \tag{38b}$$

$$U = \frac{2}{\eta}\,\mathrm{Re}(E_v E_h^*) \tag{38c}$$

$$V = \frac{2}{\eta}\,\mathrm{Im}(E_v E_h^*) \tag{38d}$$

Instead of I_v and I_h, one can also define two alternative Stokes parameters.

$$I = I_v + I_h \tag{39a}$$

$$Q = I_v - I_h \tag{39b}$$

By substituting Eqs. (32a) and (32b) into Eqs. (38a–d), we have

$$I_v = \frac{E_{v0}^2}{\eta} \tag{40a}$$

$$I_h = \frac{E_{h0}^2}{\eta} \tag{40b}$$

$$U = \frac{2}{\eta} E_{v0}E_{h0} \cos\delta \tag{40c}$$

$$V = \frac{2}{\eta} E_{v0}E_{h0} \sin\delta \tag{40d}$$

From Eqs. (39) and (40)

$$I^2 = Q^2 + U^2 + V^2 \tag{41}$$

The relation in Eq. (41) means that for elliptically polarized waves, there are only three independent parameters out of the four Stokes parameters.

$$I = \frac{E_0^2}{\eta} \tag{42}$$

$$Q = I\cos 2\chi \cos 2\psi \tag{43a}$$

$$U = I\cos 2\chi \sin 2\psi \tag{43b}$$

$$V = I\sin 2\chi \tag{43c}$$

Equations (43a) to (43c) can be conveniently expressed using the Poincare sphere (Fig. 4) with I as the radius of the sphere and Q, U, and V representing, respectively, the Cartesian axes x, y, and z. From Eqs. (43a) to (43c), it follows that 2χ is the latitude coordinate and 2ψ is the longitude coordinate. From Eqs. (43a) to (43c), Eq. (41) also follows readily. Thus, in elliptical polarization, the polarization is represented by a point on the surface of the Poincare sphere.

Partial Polarization. For fluctuating fields, the complex phasors E_v and E_h fluctuate. For random media scattering, E_v and E_h are measured for many pixels and their values fluctu-

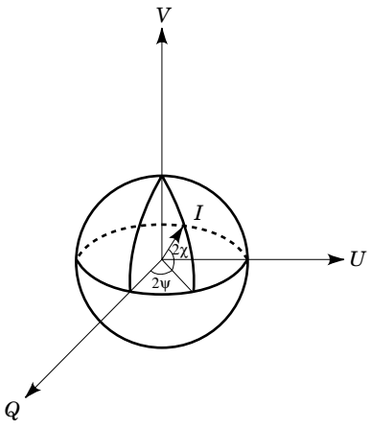

Figure 4. Poincare sphere. The north and south poles represent left-handed and right-handed circular polarization, respectively. The spherical surface represents elliptically polarized waves and the points inside the sphere represent partially polarized waves.

ate from pixel to pixel. In these cases, the Stokes parameters are defined with averages taken

$$I_v = \frac{\langle |E_v|^2 \rangle}{\eta} \tag{44a}$$

$$I_h = \frac{\langle |E_h|^2 \rangle}{\eta} \tag{44b}$$

$$U = \frac{2}{\eta} \operatorname{Re}\langle E_v E_h^* \rangle \tag{44c}$$

$$V = \frac{2}{\eta} \operatorname{Im}\langle E_v E_h^* \rangle \tag{44d}$$

Thus,

$$Q^2 + U^2 + V^2 \le I^2 \tag{45}$$

and the polarization corresponds to a point inside the Poincare sphere.

Passive Remote Sensing

Planck's Radiation Law. All substances at a finite temperature radiate electromagnetic energy. This electromagnetic radiation is measured in passive remote sensing. According to quantum theory, radiation corresponds to the transition from one energy level to another.

There are different kinds of transition, and they include electronic, vibrational, and rotational transitions. For complicated systems of molecules with an enormous number of degrees of freedom, the spectral lines are so closely spaced that the radiation spectrum becomes effectively continuous, emitting photons of all frequencies.

To derive the relation between temperature and radiated power, consider an enclosure in thermodynamic equilibrium with the radiation field it contains. The appropriate model for the radiation in the enclosure is an ideal gas of photons. Photons are governed by Bose–Einstein statistics. The procedure for finding the energy density spectrum of the radiation field consists of (a) finding the allowed modes of the enclosure, (b) finding the mean energy in each mode, and (c) finding the energy in a volume V and frequency interval $d\nu$.

We consider a dielectric medium of permittivity ϵ and dimensions a, b, and d. The dimensions a, b, and d are large enough so that we assure the fields are zero at the boundaries. We next count the modes of the medium. The mode condition is

$$\nu^2 = \frac{1}{\mu\epsilon}\left[\left(\frac{l}{2a}\right)^2 + \left(\frac{m}{2b}\right)^2 + \left(\frac{n}{2d}\right)^2\right] = \nu_x^2 + \nu_y^2 + \nu_z^2 \tag{46}$$

where l, m, and $n = 0, 1, 2, \ldots$. The number of modes in a frequency interval $d\nu$ can be determined using Eq. (46). Each set of l, m, and n corresponds to a specific cavity mode. Thus, the volume of one mode in ν space is $1/8abd(\mu\epsilon)^{3/2} = 1/8V(\mu\epsilon)^{3/2}$ with V being the physical volume of the resonator. If a quarter-hemispherical shell has a thickness $d\nu$ and radius ν, then the number of modes contained in the shell is

$$N(\nu)\,d\nu = \frac{4\pi\nu^2\,d\nu}{8} \times 8V(\mu\epsilon)^{3/2} \times 2 = 8\pi\nu^2 V\,d\nu(\mu\epsilon)^{3/2} \tag{47}$$

where the factor of 2 accounts for the existence of transverse electric field (TE) and transverse magnetic field (TM) modes. If there are n photons in a mode with frequency ν then the energy $E = nh\nu$. Using the Boltzmann probability distribution, the probability of a state with energy E is

$$P(E) = Be^{-E/KT} \tag{48}$$

where B is a normalization constant, K is Boltzmann's constant (1.38×10^{-23} J/K), and T is temperature in kelvin. Thus the average energy $\overline{E}$ in a mode with frequency ν is

$$\overline{E} = \frac{\sum_{n=0}^{\infty} EP(E)}{\sum_{n=0}^{\infty} P(E)} = \frac{\sum_{n=0}^{\infty} nh\nu e^{-nh\nu/KT}}{\sum_{n=0}^{\infty} e^{-nh\nu/KT}} = \frac{h\nu}{e^{h\nu/KT} - 1} \tag{49}$$

The amount of radiation energy per unit frequency interval and per unit volume is $w(\nu) = N(\nu)\overline{E}/V$. Hence,

$$w(\nu) = \frac{8\pi h\nu^3(\mu\epsilon)^{3/2}}{e^{h\nu/KT} - 1} \tag{50}$$

To compute radiation intensity, consider a slab of area A and infinitesimal thickness d. Such a volume would contain radiation energy

$$W = 8\pi Ad(\mu\epsilon)^{3/2}\frac{h\nu^3}{e^{h\nu/KT} - 1} \tag{51}$$

per unit frequency interval. The radiation power emerging in direction θ within solid angle $d\Omega$ is $2I\cos\theta Ad\Omega$, where I is the specific intensity per polarization and the radiation pulse will last for a time interval of $d\sqrt{\mu\epsilon}/\cos\theta$. Thus,

$$W = \int d\Omega 2AI\cos\theta\frac{d\sqrt{\mu\epsilon}}{\cos\theta} = Id\sqrt{\mu\epsilon}8\pi A \tag{52}$$

Equating Eqs. (51) and (52),

$$I = \mu\epsilon\frac{h\nu^3}{e^{h\nu/KT} - 1} \tag{53}$$

In the Rayleigh–Jean's approximation $h\nu/KT \ll 1$. This gives for a medium with permeability μ and permittivity ϵ

$$I = \frac{KT}{\lambda^2}\frac{\mu\epsilon}{\mu_0\epsilon_0} \tag{54}$$

where $\lambda = c/\nu$ is the free-space wavelength. In free space

$$I = \frac{KT}{\lambda^2} \tag{55}$$

for each polarization. The specific intensity given by Eq. (55) has dimension in power per unit area per unit frequency interval per unit solid angle ($\mathrm{W \cdot m^{-2} \cdot Hz^{-1} \cdot Sr^{-1}}$). The Rayleigh–Jean's law can be used in microwave frequencies.

Brightness Temperatures. Consider thermal emission from a half space medium of permittivity ϵ_1. In passive remote sensing, the radiometer acts as a receiver of the specific intensity I_β emitted by the medium under observation. The specific intensity is $I_\beta(\theta_0, \varphi_0)$ where β denotes the polarization and (θ_0, φ_0) denotes the angular dependence. From Eq. (54), the specific intensity inside the medium that is at temperature T is

$$I = \frac{KT}{\lambda^2}\frac{\epsilon_1}{\epsilon_0} \tag{56}$$

The specific intensity has to be transmitted through the boundary. Based on energy conservation, the received emission is,

$$I_\beta(\theta_0, \varphi_0) = \frac{KT}{\lambda^2}[1 - r_{10\beta}(\theta_1)] \tag{57}$$

In Eq. (57), $r_{10\beta}(\theta_1)$ denotes reflection when wave is incident from medium 1 onto medium 0. In Eq. (57), θ_1 and θ_0 are related by Snell's law. The measured specific intensity are often normalized to get the brightness temperatures

$$T_{B\beta}(\theta_0, \varphi_0) = I_\beta(\theta_0, \varphi_0)\frac{\lambda^2}{K} \tag{58}$$

From Eqs. (57) and (58), we obtain for a half-space medium

$$T_{B\beta}(\theta_0, \varphi_0) = T[1 - r_{10\beta}(\theta_1)] \tag{59}$$

It is convenient to define emissivity $e_\beta(\theta_0, \varphi_0)$ as

$$e_\beta(\theta_0, \varphi_0) = \frac{T_{B\beta}(\theta_0, \varphi_0)}{T} \tag{60}$$

so that

$$e_\beta(\theta_0, \varphi_0) = 1 - r_{10\beta}(\theta_1) \tag{61}$$

The reflection $r_{10\beta}$ obeys a symmetry relation that is a result of reciprocity and energy conservation.

$$r_{10\beta}(\theta_1) = r_{01\beta}(\theta_0) \tag{62}$$

where $r_{01\beta}(\theta_0)$ denote reflection for wave when incident from region 0 to region 1. Thus, emissivity is, from Eqs. (61) and (62)

$$e_\beta(\theta_0, \varphi_0) = 1 - r_{01\beta}(\theta_0) \tag{63}$$

That emissivity is equal to one minus reflectivity and is a result of energy conservation and reciprocity.

Kirchhoff's Law. Kirchhoff's law generalizes the concept of emissivity equal to one minus reflectivity to the case where there is bistatic scattering from rough surface and volume inhomogeneities.

$$e_\beta(\theta_\mathrm{i}, \varphi_\mathrm{i}) = 1 - \frac{1}{4\pi}\sum_\alpha \int_0^{\pi/2} d\theta \sin\theta \int_0^{2\pi} d\varphi \gamma_{\alpha\beta}(\theta, \varphi; \theta_\mathrm{i}, \varphi_\mathrm{i}) \tag{64}$$

The equation above is a formula that calculates the emissivity from the bistatic scattering coefficient γ. It also relates active and passive remote-sensing measurements.

Emissivity of Four Stokes Parameters. In the following, we express emissivities in terms of bistatic scattering coefficients for all four Stokes parameters. The derivation is based on the result of fluctuation-dissipation theorem (8).

$$T_{Bv}(\hat{\boldsymbol{s}}_o) = T\left[1 - \frac{1}{4\pi}\sum_{\beta=v,h}\int_0^{2\pi} d\varphi_s \int_0^{\pi/2} d\theta_s \gamma_{\beta v}(\hat{\boldsymbol{s}}, \hat{\boldsymbol{s}}_{ob})\right] \tag{65a}$$

$$T_{Bh}(\hat{\boldsymbol{s}}_o) = T\left[1 - \frac{1}{4\pi}\sum_{\beta=v,h}\int_0^{2\pi} d\varphi_s \int_0^{\pi/2} d\theta_s \gamma_{\beta h}(\hat{\boldsymbol{s}}, \hat{\boldsymbol{s}}_{ob})\right] \tag{65b}$$

$$\begin{aligned} U_B(\hat{\boldsymbol{s}}_o) &= T_{Bv}(\hat{\boldsymbol{s}}_o) + T_{Bh}(\hat{\boldsymbol{s}}_o) \\ &\quad - 2T\left[1 - \frac{1}{4\pi}\sum_{\beta=v,h}\int_0^{2\pi} d\varphi_s \int_0^{\pi/2} d\theta_s \gamma_{\beta p}(\hat{\boldsymbol{s}}, \hat{\boldsymbol{s}}_{ob})\right] \\ &= \frac{T}{4\pi}\sum_{\beta=v,h}\int_0^{2\pi} d\varphi_s \int_0^{\pi/2} d\theta_s [\gamma_{\beta p}(\hat{\boldsymbol{s}}, \hat{\boldsymbol{s}}_{ob}) - \gamma_{\beta v}(\hat{\boldsymbol{s}}, \hat{\boldsymbol{s}}_{ob}) \\ &\quad - \gamma_{\beta h}(\hat{\boldsymbol{s}}, \hat{\boldsymbol{s}}_{ob})] \end{aligned} \tag{65c}$$

$$\begin{aligned} V_B(\hat{\boldsymbol{s}}_o) &= T_{Bv}(\hat{\boldsymbol{s}}_o) + T_{Bh}(\hat{\boldsymbol{s}}_o) \\ &\quad - 2T\left[1 - \frac{1}{4\pi}\sum_{\beta=v,h}\int_0^{2\pi} d\varphi_s \int_0^{\pi/2} d\theta_s \gamma_{\beta R}(\hat{\boldsymbol{s}}, \hat{\boldsymbol{s}}_{ob})\right] \\ &= \frac{T}{4\pi}\sum_{\beta=v,h}\int_0^{2\pi} d\varphi_s \int_0^{\pi/2} d\theta_s [\gamma_{\beta R}(\hat{\boldsymbol{s}}, \hat{\boldsymbol{s}}_{ob}) \\ &\quad - \gamma_{\beta v}(\hat{\boldsymbol{s}}, \hat{\boldsymbol{s}}_{ob}) - \gamma_{\beta h}(\hat{\boldsymbol{s}}, \hat{\boldsymbol{s}}_{ob})] \end{aligned} \tag{65d}$$

In Eqs. (65), $\gamma_{\beta p}$ is the bistatic scattering coefficient of a linearly polarized wave with polarization at an angle 45° with respect to vertical and horizontal polarization wave, and $\gamma_{\beta R}$ is the bistatic scattering coefficient of an incident wave that is right-hand circular polarized. The measurement of the third and fourth Stokes parameters in microwave thermal emission from the ocean can be used to determine ocean wind (29,30).

VOLUME SCATTERING AND SURFACE SCATTERING APPROACHES

The subject of radiative transfer (7) is the analysis of radiation intensity in a medium that is able to absorb, emit, and scatter radiation. Radiative transfer theory was first initiated by Schuster in 1905 in an attempt to explain the appearance of absorption and emission lines in stellar spectra. Our inter-

est in the radiative transfer theory lies in its application to the problem of remote sensing from scattering media.

In the active and passive remote sensing of low absorption medium such as snow and ice, the effects of scattering due to medium inhomogeneities play a dominate role. Two distinct theories are being used to deal with the problem of incorporating scattering effects: wave theory and radiative transfer theory. In the wave theory, one starts out with Maxwell's equations, introduces the scattering and absorption characteristics of the medium, and tries to find solutions for the quantities of interest, such as brightness temperature, or backscattering cross sections. We take such an approach later.

Radiative transfer theory, on the other hand, starts with the radiative transfer equations that govern the propagation of energy through the scattering medium. It has an advantage in that it is simple and, more importantly, includes multiple scattering effects. Although the transfer theory was developed on the basis of radiation intensities, it contains information about the correlation of fields (9). The mutual coherence function is related to the Fourier transform of the specific intensity.

In this section, we focus on vector radiative transfer equations including the polarization characteristics of electromagnetic propagation. The extinction matrix, phase matrix, and emission vector for these two types of scattering media are obtained. The goal is to study the scattering and propagation characteristics of the Stokes parameters in radiative transfer theory and use the theory to calculate bistatic scattering cross sections and brightness temperatures.

Radiative Transfer Theory

Scalar Radiative Transfer Theory

Radiative Transfer Equation. Consider a medium, consisting of a large number of particles (Fig. 5). We have $I(\bar{r}, \hat{\boldsymbol{s}})$ at all $\bar{r}$ and for all $\hat{\boldsymbol{s}}$ due to scattering.

We consider a small volume element $dV = dAdl$, and dl is along the direction $\hat{\boldsymbol{s}}$. The small volume element is centered at $\bar{r}$. We consider the differential change in specific intensity $I(\hat{\boldsymbol{s}})$ as it passes through dV.

The differential change of power in direction $\hat{\boldsymbol{s}}$ is

$$dP = -I(\bar{r}, \hat{\boldsymbol{s}})dA\,d\Omega + I(\bar{r} + dl\hat{\boldsymbol{s}}, \hat{\boldsymbol{s}})\,dA\,d\Omega \tag{66}$$

We now look at a radiative change in a medium containing many particles. The volume dV contains many particles that are randomly positioned. The volume dV is much bigger than λ^3 so that the random phase prevails and the input and output relation of dV can be expressed in terms of intensities instead of fields.

There are three kinds of changes that will occur to $I(\bar{r}, \hat{\boldsymbol{s}})$ in the small volume element.

1. Extinction that contributes a negative change
2. Emission by the particles inside the volume dV that contributes a positive change
3. Bistatic scattering form direction $\hat{\boldsymbol{s}}'$ into direction $\hat{\boldsymbol{s}}$ that contributes a positive change

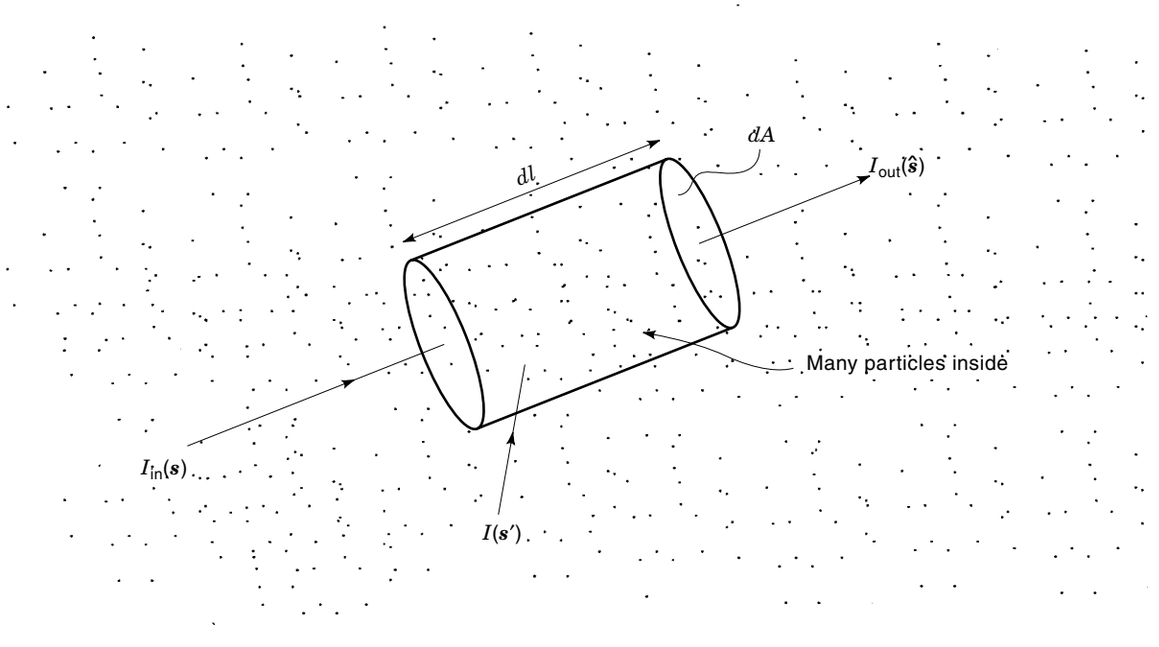

Figure 5. Specific intensity $I(\hat{\boldsymbol{s}})$ in the direction $\hat{\boldsymbol{s}}$ in and out of an elemental volume. Many particles are inside the elemental volume. Each particle absorbs power and scatters power which leads to a decrease of the specific intensity in direction $\hat{\boldsymbol{s}}$. At the same time, the specific intensity is enhanced by the emission of particles as well as the energy scattered into the direction $\hat{\boldsymbol{s}}$ from the other directions $\hat{\boldsymbol{s}}'$.

For the extinction where κ_e is the extinction cross section per unit volume of space, the differential change of power from extinction is

$$dP^{(i)} = -\kappa_e dV I(\bar{r}, \hat{\boldsymbol{s}})\, d\Omega \tag{67}$$

Let $\epsilon(\bar{r}, \hat{\boldsymbol{s}})$ be emission power per unit volume of space per unit solid angle per unit frequency; then

$$dP^{(ii)} = \epsilon(\bar{r}, \hat{\boldsymbol{s}})\, dV\, d\Omega \tag{68}$$

To derive the change due to bistatic scattering, we note that $p(\hat{\boldsymbol{s}}, \hat{\boldsymbol{s}}')$ is the bistatic scattering cross section per unit volume of space. Then if $I(\bar{r}, \hat{\boldsymbol{s}}')$ is the specific intensity in direction $\hat{\boldsymbol{s}}'$, and since $I(\bar{r}, \hat{\boldsymbol{s}}')$ exists in all directions $\hat{\boldsymbol{s}}'$,

$$dP^{(iii)} = \int_{4\pi} I(\bar{r}, \hat{\boldsymbol{s}}') d\Omega' p(\hat{\boldsymbol{s}}, \hat{\boldsymbol{s}}')\, dV\, d\Omega \tag{69}$$

where integration is over 4π directions.

Equating the sum of Eqs. (67) to (69) to Eq. (66) gives

$$\begin{aligned} -I(\bar{r}, \hat{\boldsymbol{s}})\, dA\, d\Omega + I(\bar{r} + dl\hat{\boldsymbol{s}}, \hat{\boldsymbol{s}})\, dA\, d\Omega &= \frac{dI}{ds}\, dl\, dA\, d\Omega \\ &= -\kappa_e dV I(\bar{r}, \hat{\boldsymbol{s}})\, d\Omega + \epsilon(\bar{r}, \hat{\boldsymbol{s}})\, dV\, d\Omega \\ &\quad + \int_{4\pi} I(\bar{r}, \hat{\boldsymbol{s}}')\, d\Omega' p(\hat{\boldsymbol{s}}, \hat{\boldsymbol{s}}')\, dV\, d\Omega \end{aligned} \tag{70}$$

where dI/ds is the rate of change of $I(\bar{r}, \hat{\boldsymbol{s}})$ per unit distance in direction $\hat{\boldsymbol{s}}$. Thus the radiative transfer equation with a thermal emission term at microwave frequencies is

$$\frac{d}{ds} I(\bar{r}, \hat{\boldsymbol{s}}) = -\kappa_e I(\bar{r}, \hat{\boldsymbol{s}}) + \kappa_a \frac{kT}{\lambda^2} + \int d\Omega' p(\hat{\boldsymbol{s}}, \hat{\boldsymbol{s}}') I(\bar{r}, \hat{\boldsymbol{s}}') \tag{71}$$

If one uses independent scattering, then as indicated previously, we have $\kappa_e = n_0\sigma_t$, $\kappa_a = n_0\sigma_a$, and $p(\hat{\boldsymbol{s}}, \hat{\boldsymbol{s}}') = n_0|f(\hat{\boldsymbol{s}}, \hat{\boldsymbol{s}}')|^2$.

Passive Microwave Remote Sensing of a Layer Nonscattering Medium. Passive microwave remote sensing of the earth measured the thermal emission from the atmosphere and the earth with a receiving antenna known as radiometer (Fig. 6).

Let the atmosphere and the earth be at temperatures T and T_e, respectively. Also let κ_a be the absorption coefficient of the atmosphere. We make the following assumption and observations:

1. The particles are absorptive, and absorption dominates over scattering. We thus set $p(\hat{\boldsymbol{s}}, \hat{\boldsymbol{s}}') = 0$ so that $\kappa_e = \kappa_a$.

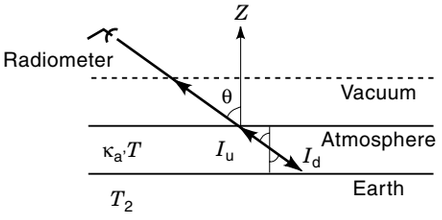

Figure 6. Thermal emission from the atmosphere and the earth. The emission is received by the receiving antenna of the radiometer.

2. $I(\bar{r}, \hat{\boldsymbol{s}}) = I(x, y, z, \theta, \varphi)$. However, by symmetry, I is independent of x, y, and φ. Thus we let $I(z, \theta)$ be the unknown.
3. Note that $I(z, \theta)$ is $0 \le \theta \le 180°$. We divide into upward- and downward-going specific intensity.

For $0 < \theta < \pi/2$

$$I_u(z, \theta) = I(z, \theta) \tag{72a}$$

$$I_d(z, \theta) = I(z, \pi - \theta) \tag{72b}$$

Since

$$\hat{\boldsymbol{s}} = \sin\theta\cos\varphi\hat{\boldsymbol{x}} + \sin\theta\sin\varphi\hat{\boldsymbol{y}} + \cos\theta\hat{\boldsymbol{z}}$$

$$\hat{\boldsymbol{s}} \cdot \overline{\nabla} I(\bar{r}, \hat{\boldsymbol{s}}) = \begin{cases} \cos\theta \dfrac{dI_u}{dz} & \text{for } I_u \\ -\cos\theta \dfrac{dI_d}{dz} & \text{for } I_d \end{cases} \tag{73}$$

Thus the radiative transfer equations become

$$\cos\theta \frac{dI_u}{dz} = -\kappa_a I_u + \kappa_a \frac{KT}{\lambda^2} \tag{74a}$$

$$-\cos\theta \frac{dI_d}{dz} = -\kappa_a I_d + \kappa_a \frac{KT}{\lambda^2} \tag{74b}$$

The boundary condition for the radiative transfer equations are as follows: At $z = 0$, top of the atmosphere

$$I_d(z = 0) = 0 \tag{75}$$

At $z = -d$, the boundary separately the atmosphere and the earth surface,

$$I_d(z = -d) = rI_d(z = -d) + \frac{KT_2}{\lambda^2}(1 - r) \tag{76}$$

where KT_2/λ^2 is the black-body specific intensity from the earth. The Fresnel reflectivity r depends on θ as well as polarization, as noted previously. The solution of Eqs. (74a) and (74b) can be expressed in terms of the sum of particular and homogeneous solutions.

$$I_u = \frac{KT}{\lambda^2} + Ae^{-\kappa_a \sec\theta z} \tag{77a}$$

$$I_d = \frac{KT}{\lambda^2} + Be^{\kappa_a \sec\theta z} \tag{77b}$$

where A and B are constants to be determined. Imposing the boundary condition [Eq. (75)] and Eq. (77b) gives

$$B = \frac{-KT}{\lambda^2}$$

and

$$\begin{aligned} A = &-\frac{KT}{\lambda^2} e^{-\kappa_a d \sec\theta} + r\frac{KT}{\lambda^2} e^{-\kappa_a d \sec\theta}(1 - e^{\kappa_a d \sec\theta}) \\ &+ \frac{KT_2}{\lambda^2}(1 - r)e^{-\kappa_a d \sec\theta} \end{aligned} \tag{78}$$

Putting Eq. (78) in Eq. (77) gives I_u. The measured specific intensity by the radiometer is $I_u(z = 0)$, and

$$I_u(z=0) = \frac{KT}{\lambda^2}(1 - e^{-\kappa_a d\sec\theta}) + \frac{KT}{\lambda^2} re^{-\kappa_a d\sec\theta}(1 - e^{\kappa_a d\sec\theta}) + \frac{KT_2}{\lambda^2}(1-r)e^{-\kappa_a d\sec\theta} \tag{79}$$

The first term is the emission of a layer of thickness d with absorption coefficient κ_a. The second term is the downward emission of the layer that is reflected by the earth. It is further attenuated as it travels upward to the radiometer. The last term is the upward emission of the earth that is attenuated by the atmosphere. It is convenient to normalize the measured I to a quantity with units of temperature. The brightness temperature T_B is defined by

$$\begin{aligned} T_B &= \frac{\text{measured } I}{K/\lambda^2} \\ &= T(1 - e^{-\kappa_a d\sec\theta}) + Tre^{-\kappa_a d\sec\theta}(1 - e^{\kappa_a d\sec\theta}) \\ &\quad + T_2(1-r)e^{-\kappa_a d\sec\theta} \end{aligned} \tag{80}$$

Vector Radiative Transfer Equation

Phase Matrix of Independent Scattering. For vector electromagnetic wave scattering, the vector radiative transfer equation has to be developed for the Stokes parameters. We first treat scattering of waves by a single particle (e.g., raindrop, ice grain, leaf, etc.). The scattering property of the particle depends on its size, shape, orientation, and dielectric properties. Consider a plane wave

$$\overline{E} = (\hat{\boldsymbol{v}}_i E_{vi} + \hat{\boldsymbol{h}}_i E_{hi}) e^{i\overline{k}_i \cdot \overline{r}} = \hat{\boldsymbol{e}}_i E_0 e^{i\overline{k}_i \cdot \overline{r}} \tag{81}$$

impinging upon the particle. In spherical coordinates

$$\hat{\boldsymbol{k}}_i = \sin\theta_i \cos\varphi_i \hat{\boldsymbol{x}} + \sin\theta_i \sin\varphi_i \hat{\boldsymbol{y}} + \cos\theta_i \hat{\boldsymbol{z}} \tag{82}$$

$$\hat{\boldsymbol{v}}_i = \cos\theta_i \cos\varphi_i \hat{\boldsymbol{x}} + \cos\theta_i \sin\varphi_i \hat{\boldsymbol{y}} - \sin\theta_i \hat{\boldsymbol{z}} \tag{83}$$

$$\hat{\boldsymbol{h}}_i = -\sin\varphi_i \hat{\boldsymbol{x}} + \cos\varphi_i \hat{\boldsymbol{y}} \tag{84}$$

In the direction $\hat{\boldsymbol{k}}_s$, the far-field scattered wave $\overline{E}_s$ will be a spherical wave and is denoted by

$$\overline{E}_s = (\hat{\boldsymbol{v}}_s E_{vs} + \hat{\boldsymbol{h}}_s E_{hs}) e^{i\overline{k}_s \cdot \overline{r}} \tag{85}$$

with

$$\hat{\boldsymbol{k}}_s = \sin\theta_s \cos\varphi_s \hat{\boldsymbol{x}} + \sin\theta_s \sin\varphi_s \hat{\boldsymbol{y}} + \cos\theta_s \hat{\boldsymbol{z}} \tag{86}$$

$$\hat{\boldsymbol{v}}_s = \cos\theta_s \cos\varphi_s \hat{\boldsymbol{x}} + \cos\theta_s \sin\varphi_s \hat{\boldsymbol{y}} - \sin\theta_s \hat{\boldsymbol{z}} \tag{87}$$

$$\hat{\boldsymbol{h}}_s = -\sin\varphi_s \hat{\boldsymbol{x}} + \cos\varphi_s \hat{\boldsymbol{y}} \tag{88}$$

The scattered field will assume the form

$$\overline{E}_s = \frac{e^{ikr}}{r} \overline{\overline{F}}(\theta_s, \varphi_s; \theta_i, \varphi_i) \cdot \hat{\boldsymbol{e}}_i E_0 \tag{89}$$

where $\overline{\overline{F}}(\theta_s, \varphi_s; \theta_i, \varphi_i)$ is the scattering function matrix. Hence

$$\begin{bmatrix} E_{vs} \\ E_{hs} \end{bmatrix} = \frac{e^{ikr}}{r} \begin{bmatrix} f_{vv}(\theta_s, \varphi_s; \theta_i, \varphi_i) & f_{vh}(\theta_s, \varphi_s; \theta_i, \varphi_i) \\ f_{hv}(\theta_s, \varphi_s; \theta_i, \varphi_i) & f_{hh}(\theta_s, \varphi_s; \theta_i, \varphi_i) \end{bmatrix} \cdot \begin{bmatrix} E_{vi} \\ E_{hi} \end{bmatrix} \tag{90}$$

with

$$f_{ab}(\theta_s, \varphi_s; \theta_i, \varphi_i) = \hat{\boldsymbol{a}}_s \cdot \overline{\overline{F}}(\theta_s, \varphi_s; \theta_i, \varphi_i) \cdot \hat{\boldsymbol{b}}_i \tag{91}$$

and $a,b = v,h$. To relate the scattered Stokes parameters to the incident Stokes parameters, we define

$$\overline{I}_s = \frac{1}{r^2} \overline{\overline{L}}(\theta_s, \varphi_s; \theta_i, \varphi_i) \cdot \overline{I}_i \tag{92}$$

where $\overline{I}_s$ and $\overline{I}_i$ are column matrices containing the scattering and incident Stokes parameters, respectively.

$$\overline{I}_s = \begin{bmatrix} I_{v_s} \\ I_{h_s} \\ U_s \\ V_s \end{bmatrix} \tag{93}$$

$$\overline{I}_i = \begin{bmatrix} I_{v_i} \\ I_{h_i} \\ U_i \\ V_i \end{bmatrix} \tag{94}$$

and $\overline{\overline{L}}(\theta_s, \varphi_s; \theta_i, \varphi_i)$ is the Stokes matrix.

$$\overline{\overline{L}}(\theta_s, \varphi_s; \theta_i, \varphi_i) = \begin{bmatrix} |f_{vv}|^2 & |f_{vh}|^2 \\ |f_{hv}|^2 & |f_{hh}|^2 \\ 2\mathrm{Re}(f_{vv} f_{hv}^*) & 2\mathrm{Re}(f_{vh} f_{hh}^*) \\ 2\mathrm{Im}(f_{vv} f_{hv}^*) & 3\mathrm{Im}(f_{vh} f_{hh}^*) \end{bmatrix} \begin{bmatrix} \mathrm{Re}(f_{vh}^* f_{vv}) & -\mathrm{Im}(f_{vh}^* f_{vv}) \\ \mathrm{Re}(f_{hh}^* f_{hv}) & -\mathrm{Im}(f_{hv} f_{hh}^*) \\ \mathrm{Re}(f_{vv} f_{hh}^* + f_{vh} f_{hv}^*) & -\mathrm{Im}(f_{vv} f_{hh}^* - f_{vh} f_{hv}^*) \\ \mathrm{Im}(f_{vv} f_{hh}^* + f_{vh} f_{hv}^*) & \mathrm{Re}(f_{vv} f_{hh}^* - f_{vh} f_{hv}^*) \end{bmatrix} \tag{95}$$

Because of the incoherent addition of Stokes parameters, the phase matrix is equal to the average of the Stokes matrix over the distribution of particles in terms of size, shape, and orientation.

Extinction Matrix. For nonspherical particles, the extinction matrix is generally nondiagonal. The extinction coefficients can be identified with the attenuation of the coherent wave, which can be calculated by using Foldy's approximation (10).

Let E_v and E_h be, respectively, the vertically and horizontally polarized components of the coherent wave. Then the following coupled equations hold for the coherent field along the propagation direction (θ, φ). Let the direction of propagation be denoted by $\hat{\boldsymbol{s}}$ with $\hat{\boldsymbol{s}}(\theta, \varphi) = \sin\theta\cos\varphi\hat{\boldsymbol{x}} + \sin\theta\sin\varphi\hat{\boldsymbol{y}} + \cos\theta\hat{\boldsymbol{z}}$.

$$\frac{dE_v}{ds} = (ik + M_{vv})E_v + M_{vh}E_h \tag{96}$$

$$\frac{dE_h}{ds} = M_{hv}E_v + (ik + M_{hh})E_h \tag{97}$$

where s is the distance along the direction of propagation. Solving Eqs. (96) and (97) yields two characteristic waves with defined polarization and attenuation rates. Thus, for propagation along any particular directions (θ, φ), there are only two attenuation rates. In Eqs. (96) and (97)

$$M_{jl} = \frac{i2\pi n_0}{k}\langle f_{jl}(\theta,\varphi;\theta,\varphi)\rangle \quad j,l = v,h \tag{98}$$

where the angular bracket denotes the average to be taken over the orientation and size distribution of the particles.

Using the definition of Stokes parameters I_v, I_h, U, and V as well as Eqs. (96) and (97), the differential equations can be derived for dI_v/ds, dI_h/ds, dU/ds, and dV/ds

$$\frac{dI_v}{ds} = 2\mathrm{Re}(M_{vv})I_v + \mathrm{Re}(M_{vh})U + \mathrm{Im}(M_{vh})V \tag{99}$$

$$\frac{dI_h}{ds} = 2\mathrm{Re}(M_{hh})I_h + \mathrm{Re}(M_{hv})U - \mathrm{Im}(M_{hv})V \tag{100}$$

$$\frac{dU}{ds} = 2\mathrm{Re}(M_{hv})I_v + 2\mathrm{Re}(M_{vh})I_h + [\mathrm{Re}(M_{vv}) + \mathrm{Re}(M_{hh})]U - [\mathrm{Im}(M_{vv}) - \mathrm{Im}(M_{hh})]V \tag{101}$$

$$\frac{dV}{ds} = -2\mathrm{Im}(M_{hv})I_v + 2\mathrm{Im}(M_{vh})I_h + [\mathrm{Im}(M_{vv}) - \mathrm{Im}(M_{hh})]U + [\mathrm{Re}(M_{vv}) + \mathrm{Re}(M_{hh})]V \tag{102}$$

Identifying the extinction coefficients in radiative transfer theory as the attenuation rates in coherent wave propagation, we have the following general extinction matrix for nonspherical particles.

$$\bar{\bar{\kappa}}_e = \begin{bmatrix} -2\mathrm{Re}\,M_{vv} & 0 & -\mathrm{Re}(M_{vh}) & -\mathrm{Im}(M_{vh}) \\ 0 & -2\mathrm{Re}\,M_{hh} & -\mathrm{Re}(M_{hv}) & \mathrm{Im}(M_{hv}) \\ -2\mathrm{Re}\,M_{hv} & -2\mathrm{Re}\,M_{vh} & -(\mathrm{Re}\,M_{vv} + \mathrm{Re}\,M_{hh}) & (\mathrm{Im}\,M_{vv} - \mathrm{Im}\,M_{hh}) \\ 2\mathrm{Im}\,M_{hv} & -2\mathrm{Im}\,M_{vh} & -(\mathrm{Im}\,M_{vv} - \mathrm{Im}\,M_{hh}) & -(\mathrm{Re}\,M_{vv} + \mathrm{Re}\,M_{hh}) \end{bmatrix} \tag{103}$$

Emission Vector. In this section, we list the emission vector for passive remote sensing of nonspherical particles. The fluctuation–dissipation theorem is used to calculate the emission of a single nonspherical particle. Generally, all four Stokes parameters in the vector source term are nonzero and are proportional to the absorption coefficient in the backward direction (11).

The emission term can be inserted into the vector radiative transfer equations, which assume the following form

$$\frac{d\bar{I}(\bar{r},\hat{s})}{ds} = -\bar{\bar{\kappa}}_e(\hat{s})\cdot\bar{I}(\bar{r},\hat{s}) + \bar{\bar{r}}(\hat{s})CT(\bar{r}) + \int d\Omega'\bar{\bar{P}}(\hat{s},\hat{s}')\cdot\bar{I}(\bar{r},\hat{s}) \tag{104}$$

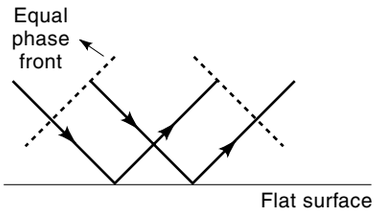

Figure 7. Waves reflected by a flat surface. The reflected waves have the same phase in the specular direction.

where $\bar{\bar{\kappa}}_e(\hat{s})$ is the extinction matrix and $\bar{\bar{P}}(\hat{s},\hat{s}')$ is the phase matrix.

$$\bar{\bar{r}}(\hat{s}) = \begin{bmatrix} \kappa_{a1}(\hat{s}) \\ \kappa_{a2}(\hat{s}) \\ -\kappa_{a3}(\hat{s}) \\ -\kappa_{a4}(\hat{s}) \end{bmatrix} \tag{105}$$

$$\kappa_{a1}(\hat{s}) = \kappa_{e11}(\hat{s}) - \int d\Omega'[P_{11}(\hat{s}',\hat{s}) + P_{21}(\hat{s}',\hat{s})] \tag{106a}$$

$$\kappa_{a2}(\hat{s}) = \kappa_{e22}(\hat{s}) - \int d\Omega'[P_{12}(\hat{s}',\hat{s}) + P_{22}(\hat{s}',\hat{s})] \tag{106b}$$

$$\kappa_{a3}(\hat{s}) = 2\kappa_{e13}(\hat{s}) + 2\kappa_{e23}(\hat{s}) - 2\int d\Omega'[P_{13}(\hat{s}',\hat{s}) + P_{23}(\hat{s}',\hat{s})] \tag{106c}$$

$$\kappa_{a4}(\hat{s}) = -2\kappa_{e14}(\hat{s}) - 2\kappa_{e24}(\hat{s}) + 2\int d\Omega'[P_{14}(\hat{s}',\hat{s}) + P_{24}(\hat{s}',\hat{s})] \tag{106d}$$

where κ_{eij} and P_{ij} are, respectively, the ij elements of $\bar{\bar{\kappa}}_e$ and $\bar{\bar{P}}$ with $i, j = 1, 2, 3$, or 4.

The vector radiative transfer theory has been applied extensively to microwave remote sensing problems (2,5,12).

Random Rough Surface Scattering

Consider a plane wave incident on a flat surface (Fig. 7). We note that the wave is specularly reflected because the specular reflected waves are in phase with each other. The reflected wave only exists in the specular direction. Imagine now that the surface is rough. It is clear from Fig. 8 that the two reflected waves have a pathlength difference of $2h\cos\theta_i$. This will give a phase difference of

$$\Delta\varphi = 2kh\cos\theta_i \tag{107}$$

If h is small compared with a wavelength, then the phase difference is insignificant. However, if the phase difference is significant, the specular reflection will be reduced due to interference of the reflected waves that can partially cancel each other. The scattered wave is diffracted into other direc-

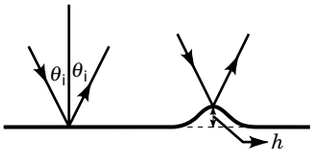

Figure 8. Waves scattered by a rough surface. Two reflected waves have a pathlength difference of $2h\cos\theta_i$ that lead to a phase difference of $\Delta\varphi = 2kh\cos\theta_i$.

tions. A Rayleigh condition is defined such that the phase difference is 90°. Thus for

$$h < \frac{\lambda}{8}\cos\theta_{\mathrm{i}} \tag{108}$$

the surface is regarded as smooth and if

$$h > \frac{\lambda}{8}\cos\theta_{\mathrm{i}} \tag{109}$$

the surface is regarded as rough. For random rough surface, h is regarded as the root mean square (rms) height.

Consider an incident wave $\psi_{\mathrm{inc}}(\bar{r})$ impinging upon a rough surface. The wave function ψ obeys the wave equation:

$$(\nabla^2 + k^2)\psi = 0 \tag{110}$$

The rough surface is described by a height function $z = f(x, y)$. Two common boundary conditions are those of the Dirichlet problem and the Neumann problem. For the Dirichlet problem, at $z = f(x, y)$

$$\psi = 0 \tag{111}$$

For the Neumann problem, the boundary condition is at $z = f(x, y)$

$$\partial\psi/\partial n = 0 \tag{112}$$

where $\partial\psi/\partial n$ is the normal derivative.

In this section, we illustrate the analytic techniques for scattering by such surfaces. For electromagnetic wave scattering by a one-dimensional rough surface $z = f(x)$, the Dirichlet problem corresponds to that of a TE wave impinging upon a perfect conductor, where ψ is the electric field. The Neumann problem corresponds to that of a TM wave impinging upon a perfect electric conductor and ψ is the magnetic field. In the section on numerical simulations, the cases of dielectric surfaces are simulated. The simplified perfect conductor has been used in studying active remote sensing of the ocean that is reflective to electromagnetic waves.

Statistics, Correlation Function, and Spectral Density. For a one-dimensional random rough surface, we let $z = f(x)$, where $f(x)$ is a random function of x with zero mean

$$\langle f(x)\rangle = 0 \tag{113}$$

We define the Fourier transform

$$F(k_x) = \frac{1}{2\pi}\int_{-\infty}^{\infty} dx e^{-ik_x x} f(x) \tag{114}$$

Strictly speaking, if the surface is infinite, the Fourier transform does not exist. To circumvent the difficulty one can use the Fourier Stieltjes integral (1), or one can define truncated function

$$f_L(x) = \begin{cases} f(x) & |x| \le L/2 \\ 0 & |x| \ge L/2 \end{cases} \tag{115}$$

The Fourier transform then becomes

$$F_L(k_x) = \frac{1}{2\pi}\int_{-\infty}^{\infty} dx e^{-ik_x x} f_L(x) \tag{116}$$

The two sets [Eqs. (114) and (116)] should agree for large L. Physically, the domain of the rough surface is always limited by the antenna beamwidth.

For a stationary random process

$$\langle f(x_1) f(x_2)\rangle = h^2 C(x_1 - x_2) \tag{117}$$

where h is the rms height and C is the correlation function. Some commonly used correlation functions are Gaussian correlation function

$$C(x) = \exp(-x^2/l^2) \tag{118}$$

and exponential correlation function

$$C(x) = \exp(-|x|/l) \tag{119}$$

In Eqs. (118) and (119) l is known as the correlation length.

In the spectral domain

$$\langle F(k_x)\rangle = 0 \tag{120}$$

and

$$h^2 C(x_1 - x_2) = \int_{-\infty}^{\infty} dk_{1x}\int_{-\infty}^{\infty} dk_{2x} e^{ik_{1x}x_1 - ik_{2x}x_2}\langle F(k_{1x})F^*(k_{2x})\rangle \tag{121}$$

Since the left-hand side depends only on $x_1 - x_2$, we have

$$\langle F(k_{1x})F^*(k_{2x})\rangle = \langle F(k_{1x})F(-k_{2x})\rangle = \delta(k_{1x} - k_{2x})W(k_{1x}) \tag{122}$$

and

$$h^2 C(x) = \int_{-\infty}^{\infty} dk_x e^{ik_x x} W(k_x) \tag{123}$$

where $W(k_x)$ is known as the spectral density. Since $f(x)$ is real, we have used the relation.

$$F^*(k_x) = F(-k_x) \tag{124}$$

Since

$$C(x) = C(-x) \tag{125}$$

and $C(x)$ is real, it follows that $W(k_x)$ is real and is an even function of k_x. Instead of using a correlation function to describe the Gaussian random process, one can also use the spectral density.

For Gaussian correlation function of Eq. (118)

$$W(k_x) = \frac{h^2 l}{2\sqrt{\pi}}\exp\left(-\frac{k_x^2 l^2}{4}\right) \tag{126}$$

and for exponential correlation of Eq. (119)

$$W(k_x) = \frac{h^2 l}{\pi(1 + k_x^2 l^2)} \tag{127}$$

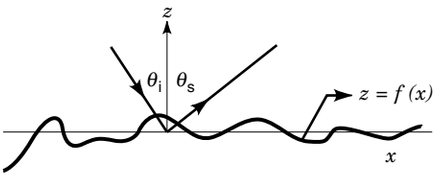

Figure 9. The wave scattering from a slightly rough surface. The incident and scattered directions and the rough surface profile are shown.

Small Perturbation Method. The scattering of electromagnetic waves from a slightly rough surface can be studied using a perturbation method (9). It is assumed that the surface variations are much smaller than the incident wavelength and the slopes of the rough surface are relatively small. The small perturbation method (SPM) makes use of the Rayleigh hypothesis to express the reflected and transmitted fields into upward- and downward-going waves, respectively. The field amplitudes are then determined from the boundary conditions. An investigation of the validity of the Rayleigh hypothesis can be found in Ref. 13. A renormalization method can also be used to make corrections on the small perturbation method (14,15). In this section, we use the small perturbation method to carry out scattering up to second order and show that energy conservation is exactly obeyed. The incoherent wave is calculated up to first order to obtain bistatic scattering coefficients.

Dirichlet Problem for One-Dimensional Surface. We first illustrate the method for a simple one-dimensional random rough surface with height profile $z = f(x)$ and $\langle f(x)\rangle = 0$. The scattering is a two-dimensional problem in $x - z$ without y variation.

Consider an incident wave impinging on such a surface with the Dirichlet boundary condition (Fig. 9). Let

$$E_{\text{inc}} = e^{ik_{\text{ix}}x - ik_{\text{iz}}z} \tag{128}$$

where $k_{\text{ix}} = k \sin\theta_{\text{i}}$, $k_{\text{iz}} = k\cos\theta_{\text{i}}$. In the perturbation method, one uses the height of the random rough surface as a small parameter. We assume that $kh \ll 1$, where h is the rms height.

For the scattered wave, we write it as a perturbation series.

$$E_{\text{s}} = E_{\text{s}}^{(0)} + E_{\text{s}}^{(1)} + E_{\text{s}}^{(2)} + \cdots \tag{129}$$

The boundary condition at $z = f(x)$ is

$$E_{\text{inc}} + E_{\text{s}} = 0 \tag{130}$$

The zeroth order scattered wave is the reflection from a flat surface at $z = 0$. Thus

$$E_{\text{s}}^{(0)} = -e^{ik_{\text{ix}}x + ik_{\text{iz}}z} \tag{131}$$

We let the scattered field to be represented by

$$E_{\text{s}}(\bar{r}) = \int_{-\infty}^{\infty} dk_x e^{ik_x x + ik_z z} E_{\text{s}}(k_x) \tag{132}$$

where $k_z = (k^2 - k_x^2)^{1/2}$. The Rayleigh hypothesis (13) has been invoked in Eq. (132) as the scattered wave is expressed in terms of a spectrum of upward plane waves only. To calculate $E_{\text{s}}(k_x)$, we match the boundary condition from Eq. (130),

$$e^{ik_{\text{ix}}x - ik_{\text{iz}}f(x)} + \int_{-\infty}^{\infty} dk_x e^{ik_x x + ik_z z} E_{\text{s}}(k_x) = 0 \tag{133}$$

Perturbation theory consists of expanding the exponential functions of $\exp[-ik_{iz}f(x)]$ and $\exp[ik_z f(x)]$ in power series. In the spectral domain, we also let

$$E_{\text{s}}(k_x) = E_{\text{s}}^{(0)}(k_x) + E_{\text{s}}^{(1)}(k_x) + E_{\text{s}}^{(2)}(k_x) + \cdots \tag{134}$$

Thus assuming that $|k_z f(x)| \ll 1$

$$\begin{aligned} e^{ik_{\text{ix}}x}\left[1 - ik_{\text{iz}}f(x) - \frac{k_{\text{iz}}^2 f^2(x)}{2} + \cdots\right] \\ + \int_{-\infty}^{\infty} dk_x e^{ik_x x}\left[1 + ik_z f(x) - \frac{k_z^2 f^2(x)}{2} + \cdots\right] \\ \times [E_{\text{s}}^{(0)}(k_x) + E_{\text{s}}^{(1)}(k_x) + E_{\text{s}}^{(2)}(k_x) + \cdots] = 0 \end{aligned} \tag{135}$$

Balancing Eq. (135) to zeroth order gives

$$e^{ik_{\text{ix}}x} + \int_{-\infty}^{\infty} dk_x e^{ik_x x} E_s^{(0)}(k_x) = 0 \tag{136}$$

so that

$$E_{\text{s}}^{(0)}(k_x) = -\delta(k_x - k_{\text{ix}}) \tag{137}$$

If we substitute Eq. (137) into Eq. (132), we get back the zeroth order solution in the space domain as given by Eq. (131).

Balancing Eq. (135) to first order gives,

$$\begin{aligned} -e^{ik_{\text{ix}}x}[ik_{\text{iz}}f(x)] + \int_{-\infty}^{\infty} dk_x e^{ik_x x}[ik_z f(x)]E_{\text{s}}^{(0)}(k_x) \\ = -\int_{-\infty}^{\infty} dk_x e^{ik_x x} E_{\text{s}}^{(1)}(k_x) \end{aligned} \tag{138}$$

From Eq. (138), it follows that the first-order solution can be expressed in terms of the zeroth-order solution. Substituting Eq. (137) in Eq. (138) gives

$$\begin{aligned} \int_{-\infty}^{\infty} dk_x e^{ik_x x} E_{\text{s}}^{(1)}(k_x) &= 2ik_{\text{iz}}f(x)e^{ik_x x} \\ &= 2ik_{\text{iz}}\int_{-\infty}^{\infty} dk_x F(k_x) e^{ik_x x + ik_{\text{ix}}x} \end{aligned} \tag{139}$$

The second equality is a result of using the Fourier transform of $f(x)$ from Eq. (114). Thus

$$E_{\text{s}}^{(1)}(k_x) = 2ik_{\text{iz}}F(k_x - k_{\text{ix}}) \tag{140}$$

The result of Eq. (140) can be interpreted as follows. For the wave to be scattering from incident direction k_{ix} to scattered direction k_x, the surface has to provide the spectral component

of $k_x - k_{ix}$. This is characteristic of Bragg scattering. Balancing Eq. (135) to second order gives

$$e^{ik_{ix}x}\frac{k_{iz}^2 f^2(x)}{2} + \int_{-\infty}^{\infty} dk_x e^{ik_x x}\left[\frac{k_z^2 f^2(x)}{2} E_s^{(0)}(k_x)\right] - \int_{-\infty}^{\infty} dk_x e^{ik_x x} ik_z f(x) E_s^{(1)}(k_x) = \int_{-\infty}^{\infty} dk_x e^{ik_x x} E_s^{(2)}(k_x) \quad (141)$$

Using Eq. (137), the first two terms in Eq. (141) canceled each other. Thus the second-order solution can be expressed in terms of the zeroth-order and first-order solutions. Substituting Eqs. (140) and (137) in Eq. (141) gives the second-order solution

$$E_s^{(2)}(k_x) = 2\int_{-\infty}^{\infty} dk_x' k_z' k_{iz} F(k_x - k_x') F(k_x' - k_{ix}) \quad (142)$$

where $k_z' = (k^2 - k_x'^2)^{1/2}$. Equation (142) has the following simple physical interpretation. Second-order scattering consists of scattering from the incident direction k_{ix} into an intermediate direction k_x' as provided by spectral component $k_x' - k_{ix}$ of the rough surface. This is followed by another scattering from k_x' to direction k_x as provided by spectral component $k_x - k_x'$ of the rough surface. Since k_x' is an arbitrary direction, an integration over all possible k_x' is needed in Eq. (142).

Coherent Wave Reflection. The coherent wave is obtained by calculating the stochastic average. We note that,

$$\langle E_s^{(1)}(k_x)\rangle = 0 \quad (143)$$

$$\langle E_s^{(2)}(k_x)\rangle = 2\delta(k_x - k_{ix}) k_{iz} \int_{-\infty}^{\infty} dk_x' k_z' W(k_{ix} - k_x') \quad (144)$$

The dirac function $\delta(k_x - k_{ix})$ in Eqs. (137) and (144) indicate that the coherent wave is in the specular direction. Substituting Eqs. (137), (143) and (144) in Eq. (132) gives the coherent field, to second order,

$$\langle E_s(\bar{r})\rangle = \langle E_s^{(0)}(\bar{r})\rangle + \langle E_s^{(2)}(\bar{r})\rangle \quad (145)$$

$$\langle E_s^{(0)}(\bar{r})\rangle = -e^{ik_{ix}x + ik_{iz}z} \quad (146)$$

$$\langle E_s^{(2)}(\bar{r})\rangle = e^{ik_{ix}x + ik_{iz}z} 2k_{iz} \int_{-\infty}^{\infty} dk_x k_z W(k_{ix} - k_x) \quad (147)$$

Because the two terms in Eq. (145) are opposite in signs, the result of Eq. (145) indicates that the coherent reflection is less than that of the flat-surface case.

Bistatic Scattering. To study energy transfer in scattering, we note that incident wave has power per unit area

$$\overline{S}_{inc} \cdot \hat{\boldsymbol{z}} = -\frac{1}{2\eta}\cos\theta_i \quad (148)$$

flowing into the rough surface, where η is the wave impedance. The negative sign in Eq. (148) indicates that the Poynting vector has a negative $\hat{\boldsymbol{z}}$ component.

The power per unit area outflowing from the rough surface is

$$\langle \overline{S}_s \cdot \hat{\boldsymbol{z}}\rangle = \mathrm{Re}\left(\frac{i}{2\omega\mu}\left\langle E_s \frac{\partial E_s^*}{\partial z}\right\rangle\right) \quad (149)$$

Suppose we include up to $E_s^{(0)}E_s^{(0)*} + \langle E_s^{(1)}E_s^{(1)*}\rangle + E_s^{(0)}\langle E_s^{(2)*}\rangle + \langle E_s^{(2)}\rangle E_s^{(0)*}$ in Eq. (149). That is, we include the intensity due to the product of first-order fields and the product of the zeroth-order field and the second-order field. Thus the power per unit area outflowing from the rough surface that is associated with the coherent field $\langle \overline{S} \cdot \hat{\boldsymbol{z}}\rangle_C$ is

$$\langle \overline{S}_s \cdot \hat{\boldsymbol{z}}\rangle_C = \mathrm{Re}\left(\frac{i}{2\omega\mu}\langle E_s^{(0)}(\bar{r})\rangle \frac{\partial}{\partial z}\langle E_s^{(0)}(r)\rangle + \langle E_s^{(0)}(r)\rangle \frac{\partial}{\partial z}\langle E_s^{(2)*}(\bar{r})\rangle + \langle E_s^{(2)}(r)\rangle \frac{\partial}{\partial z}\langle E_s^{(0)*}(\bar{r})\rangle\right) \quad (150)$$

Putting Eqs. (145) to (147) into Eq. (150) gives

$$\langle \overline{S}_s \cdot \hat{\boldsymbol{z}}\rangle_C = \frac{k_{iz}}{2\omega\mu}\left\{1 - 4k_{iz}\int_{-\infty}^{\infty} dk_x (\mathrm{Re}\, k_z) W(k_{ix} - k_x)\right\} \quad (151)$$

Note that W, the spectra density, is real. Since k_z is imaginary for evanescent waves, the integration limits of Eq. (151) are replaced by $-k$ to k, because k_z is imaginary for the evanescent waves and the integrand does not contribute. This means that evanescent waves do not contribute to the average power flow.

$$\langle \overline{S}_s \cdot \hat{\boldsymbol{z}}\rangle_C = \frac{\cos\theta_i}{2\eta}\left\{1 - 4k_{iz}\int_{-k}^{k} dk_x k_z W(k_{ix} - k_x)\right\} \quad (152)$$

For the incoherent wave power flow, we use the first-order scattering fields. In the spectral domain, we have the incoherent field $\langle \overline{S} \cdot \hat{\boldsymbol{z}}\rangle_{IC}$

$$\langle \overline{S}_s \cdot \hat{\boldsymbol{z}}\rangle_{IC} = \mathrm{Re}\left[\frac{1}{2\omega\mu}\int_{-\infty}^{\infty} dk_x \int_{-\infty}^{\infty} dk_x' e^{i(k_x - k_x')x} k_z'^* e^{i(k_x - k_x'^*)z} \langle E_s^{(1)}(k_x) E_s^{(1)^*}(k_x'^*)\rangle\right] \quad (153)$$

Since

$$\langle E_s^{(1)}(k_x) E_s^{(1)^*}(k_x')\rangle = 4k_{iz}^2 W(k_x - k_{ix})(k_x - k_x') \quad (154)$$

It then follows that

$$\langle \overline{S}_s \cdot \hat{\boldsymbol{z}}\rangle_{IC} = \frac{2\cos\theta_i}{\eta} k_{iz} \int_{-k}^{k} dk_x k_z W(k_x - k_{ix}) \quad (155)$$

Comparing Eq. (155) with Eq. (152) shows that the incoherent power flow exactly cancels the second term of Eq. (152) giving the relation

$$\langle \overline{S}_s \cdot \hat{\boldsymbol{z}}\rangle = \frac{\cos\theta_i}{2\eta} \quad (156)$$

that exactly obeys energy conservation. Thus if we define the incoherent wave

$$\epsilon_s = E_s - \langle E_s \rangle \tag{157}$$

$$\langle \epsilon_s(k_x)\epsilon_s^*(k_x')\rangle = \mathrm{I}(k_x)\delta(k_x - k_x') \tag{158}$$

We define the power flow per unit area of the incoherent wave as

$$\langle \overline{S}_s \cdot \hat{z}\rangle = \frac{1}{2\omega\mu}\int_{-k}^{k} dk_x k_z \mathrm{I}(k_x) \tag{159}$$

Casting in terms of angular integration, we let

$$k_x = k\sin\theta_s \tag{160}$$

$$k_z = k\cos\theta_s \tag{161}$$

$$\langle \overline{S}_s \cdot \hat{z}\rangle = \frac{k}{2\eta}\int_{\pi/2}^{\pi/2} d\theta_s \cos^2\theta_s \mathrm{I}(k_x = k\sin\theta_s) \tag{162}$$

Thus if we divide Eq. (162) by the incident power per unit area of Eq. (148), we can define the incoherent bistatic scattering coefficients.

$$\sigma(\theta_s) = \frac{k\cos^2\theta_s}{\cos\theta_i}\mathrm{I}(k_x = k\sin\theta_s) \tag{163}$$

Note that the integration of $\sigma(\theta_s)$ over θ_s will combine with the reflected power of the coherent wave to give an answer that obeys energy conservation.

For first-order scattering, $\epsilon_s^{(1)}(k_x) = E_s^{(1)}(k_x)$, so that from Eqs. (155) and (158)

$$\mathrm{I}(k_x) = 4k_{iz}^2 W(k_x - k_{ix}) \tag{164}$$

and Eq. (163) assumes the form

$$\sigma(\theta_s) = 4k^3\cos^2\theta_s\cos\theta_i W(k\sin\theta_s - k\sin\theta_i) \tag{165}$$

The backscattering coefficient is for $\theta_s = -\theta_i$

$$\sigma(-\theta_i) = 4k^3\cos^3\theta_i W(-2k\sin\theta_i) \tag{166}$$

The small perturbation method has been used for the three-dimensional scattering problem (2,4) and also for dielectric surfaces. It has been used extensively for rough surface scattering problems in soils and ocean scattering (2,12).

MONTE-CARLO SIMULATIONS OF WAVE SCATTERING FROM DENSE MEDIA AND ROUGH SURFACES

Scattering of Electromagnetic Waves from Dense Distributions of Nonspherical Particles Based on Monte Carlo Simulations

For wave propagation in a medium consisting of randomly distributed scatterers, the classical assumption is that of independent scattering, which states that the extinction rate is equal to $n_0\sigma_e$ where n_0 is the number of particles per unit volume and σ_e is the extinction cross section of one particle. This classical assumption is not valid for a dense medium that contains particles occupying an appreciable fractional volume. This has been demonstrated in controlled laboratory experiments (16). Well-known analytical approximations in multiple-scattering theory include Foldy's approximation, the quasicrystalline approximation (QCA), and the quasicrystalline approximation with coherent potential (QCA-CP) (2). The last two approximations depend on the pair distribution function of particles positions in which the Percus–Yevick (PY) approximation is used to describe the correlation of positions of particles of finite sizes (2,17).

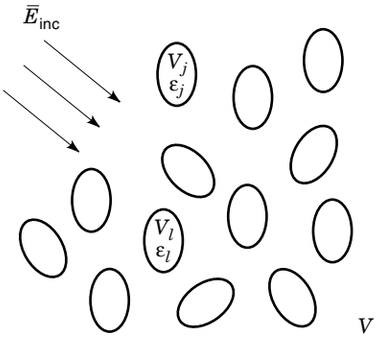

Figure 10. An incident field $\overline{E}_{inc}(\overline{r})$ incidents upon N nonoverlap, small spheroids that are randomly positioned and oriented in a volume V.

Because of the recent advent of computers and computational methods, the study of scattering by dense media has recently relied on exact solutions of Maxwell's equations through Monte Carlo simulations. Such simulations can be done by packing several thousands of particles randomly in a box, and then solving Maxwell's equations. The simulations are performed over many samples (realizations) and the scattering results are averaged over these realizations. The results give information about the collective scattering effects of many particles closely packed together.

Formulation. Let an incident electric field $\overline{E}_{inc}(\overline{r})$ impinge upon N number of randomly positioned small spheroids (Fig. 10). Spheroid j is centered at r_j and has permittivity ϵ_j, $j = 1, 2, 3, \ldots, N$. The discrete scatterers are embedded in a background with permittivity ϵ. Particle j occupies region V_j. Let $\epsilon_p(\overline{r})$ be the permittivity as a function of $\overline{r}$,

$$\epsilon_p(\overline{r}) = \begin{cases} \epsilon_j & \text{for } \overline{r} \text{ in } V_j \\ \epsilon & \text{for } \overline{r} \text{ in the background} \end{cases} \tag{167}$$

Thus the induced polarization is

$$\overline{P}(\overline{r}) = \epsilon\chi(\overline{r})\overline{E}(\overline{r}) \tag{168}$$

where

$$\chi(\overline{r}) = \frac{\epsilon_p(\overline{r})}{\epsilon} - 1 \tag{169}$$

is the electric susceptibility. The total electric field can be expressed in terms of the volume integral equation as

$$\overline{E}(\overline{r}) = \overline{E}_{inc}(\overline{r}) + k^2\int d\overline{r}'\frac{g(\overline{r},\overline{r}')}{\epsilon}\overline{P}(\overline{r}') - \overline{\nabla}\int d\overline{r}'\frac{\overline{\nabla}' g(\overline{r},\overline{r}')}{\epsilon}\overline{P}(\overline{r}') \tag{170}$$

where

$$g(\bar{r},\bar{r}') = \frac{e^{ik|\bar{r}-\bar{r}'|}}{4\pi|\bar{r}-\bar{r}'|} \tag{171}$$

is the scalar Green's function with wavenumber of the background medium $k = \omega\sqrt{\mu\epsilon}$. The induced polarization $\bar{P}(\bar{r})$ is nonzero over the particles only. Let $\bar{P}_j(\bar{r})$ be the polarization density inside the particle j. Then the volume integral equation [Eq. (170)] becomes

$$\begin{aligned}\bar{E}(\bar{r}) =& \bar{E}_{\text{inc}}(\bar{r}) + k^2 \sum_{j=1}^{N} \int_{V_j} d\bar{r}' \frac{g(\bar{r},\bar{r}')}{\epsilon} \bar{P}_j(\bar{r}') \\ &- \sum_{j=1}^{N} \bar{\nabla} \int_{V_j} d\bar{r}' \frac{\bar{\nabla}' g(\bar{r},\bar{r}')}{\epsilon} \bar{P}_j(\bar{r}')\end{aligned} \tag{172}$$

To solve Eq. (172) by the method of moments (18), we expand the electric field $\bar{E}_j(\bar{r})$ inside the jth spheroid in a set of N_b basis functions

$$\bar{E}_j(\bar{r}) = \sum_{\alpha=1}^{N_b} a_{j\alpha} \bar{f}_{j\alpha}(\bar{r}) \tag{173}$$

Here the spheroid is assumed to be small, we choose the basis functions in Eq. (173) to be the electrostatic solution of that of a spheroid.

Let the jth spheroid be centered at r_j with

$$\bar{r}_j = x_j\hat{\boldsymbol{x}} + y_j\hat{\boldsymbol{y}} + z_j\hat{\boldsymbol{z}} \tag{174}$$

and the symmetry axes of the spheroid be $\hat{\boldsymbol{x}}_{bj}$, $\hat{\boldsymbol{y}}_{bj}$, and $\hat{\boldsymbol{z}}_{bj}$, with respective semiaxes lengths be a_j, b_j, and c_j. The orientation of the symmetry axis $\hat{\boldsymbol{z}}_{bj}$ is

$$\hat{\boldsymbol{z}}_{bj} = \sin\beta_j\cos\alpha_j\hat{\boldsymbol{x}} + \sin\beta_j\sin\alpha_j\hat{\boldsymbol{y}} + \cos\beta_j\hat{\boldsymbol{z}} \tag{175}$$

The first three normalized basis functions for electric fields are

$$\bar{f}_{j1} = \hat{\boldsymbol{z}}_{bj}\frac{1}{\sqrt{v_{0j}}} \tag{176}$$

$$\bar{f}_{j2} = \hat{\boldsymbol{x}}_{bj}\frac{1}{\sqrt{v_{0j}}} \tag{177}$$

$$\bar{f}_{j3} = \hat{\boldsymbol{y}}_{bj}\frac{1}{\sqrt{v_{0j}}} \tag{178}$$

The three basis functions are those of the dipole solutions, which are constant vectors. In Eqs. (176) to (178), $v_{0j} = 4\pi a_j^2 c_j/3$. If the particles are closely packed, the near-field interactions have large spatial variations over the size of a spheroid that may induce quadrupole fields inside the spheroid. However, the non-near-field interactions have small spatial variations over the size of a spheroid and only induce dipole fields inside the spheroid.

Substituting Eqs. (173) into (172), we get

$$\bar{E}(\bar{r}) = \bar{E}_{\text{inc}}(\bar{r}) + \sum_{j=1}^{N}\sum_{\alpha=1}^{N_b} a_{j\alpha}\bar{q}_{j\alpha}(\bar{r}) \tag{179}$$

where

$$\begin{aligned}\bar{q}_{j\alpha}(\bar{r}) =& k^2 \int_{V_j} d\bar{r}' g(\bar{r},\bar{r}')\bar{f}_{j\alpha}(\bar{r}')(\epsilon_{rj}-1) \\ &- \bar{\nabla}\int_{V_j} d\bar{r}'\bar{\nabla}' g(\bar{r},\bar{r}')\cdot\bar{f}_{j\alpha}(\bar{r}')(\epsilon_{rj}-1)\end{aligned} \tag{180}$$

is the electric field induced by the polarization $\bar{P}_j(\bar{r})$ of the spheroid j. Of particular importance is the internal field created by $\bar{P}_j(\bar{r})$ on itself. Because of the smallness of the spheroid, an electrostatic solution can be sought and we have, for $\bar{r}$ in V_j

$$\bar{q}_{j\alpha}(\bar{r}) \cong C_{j\alpha}\bar{f}_{j\alpha}(\bar{r}) \tag{181}$$

where j is the particle index and α is the basis function index (19) and

$$\begin{aligned}C_{j1} &= -\frac{\epsilon_p-\epsilon}{\epsilon}\left[\frac{\xi_0}{2}\ln\left(\frac{\xi_0+1}{\xi_0-1}\right)-1\right](\xi_0^2-1) \\ C_{j2} = C_{j3} &= -\frac{1}{2}\frac{\epsilon_p-\epsilon}{\epsilon}\xi_0\left[\xi_0 - \frac{\xi_0^2-1}{2}\ln\left(\frac{\xi_0+1}{\xi_0-1}\right)\right]\end{aligned}$$

The coefficients $C_{j\alpha}$, $\alpha = 1, 2, 3$, are constants depending on particle size, shape, and permittivity. An approximation sign is used in Eq. (181) to indicate the low-frequency approximation.

Next, we apply Galerkin's method (18) to Eq. (179)

$$\begin{aligned}a_{j\beta} &= \int_{V_l} d\bar{r}\bar{f}_{l\beta}(\bar{r})\cdot\bar{E}(\bar{r}) \\ &= \int_{V_l} d\bar{r}\bar{f}_{l\beta}(\bar{r})\cdot\sum_{\alpha=1}^{N_b} a_{l\alpha}\bar{f}_{l\alpha}(\bar{r}) \\ &= \int_{V_l} d\bar{r}\bar{f}_{l\beta}(\bar{r})\cdot\bar{E}_{\text{inc}}(\bar{r}) + \sum_{\substack{j=1\\ j\neq 1}}^{N}\sum_{\alpha=1}^{N_b} a_{j\alpha}\int_{V_l} d\bar{r}\bar{f}_{l\beta}(\bar{r})\cdot\bar{q}_{j\alpha}(\bar{r}) \\ &\quad + \sum_{\alpha=1}^{N_b} a_{l\alpha}\int_{V_l} d\bar{r}\bar{f}_{l\beta}(\bar{r})\cdot\bar{q}_{l\alpha}(\bar{r}) \\ &= \int_{V_l} d\bar{r}\bar{f}_{l\beta}(\bar{r})\cdot\bar{E}_{\text{inc}}(\bar{r}) + \sum_{\substack{j=1\\ j\neq 1}}^{N}\sum_{\alpha=1}^{N_b} a_{j\alpha}\int_{V_l} d\bar{r}\bar{f}_{l\beta}(\bar{r}) \\ &\quad \cdot\bar{q}_{j\alpha}(\bar{r}) + a_{l\beta}C_{l\beta}\end{aligned} \tag{182}$$

This gives

$$\begin{aligned}a_{l\beta} = \frac{1}{(1-C_{l\beta})}\Bigg\{&\int_{V_l} d\bar{r}\bar{f}_{l\beta}(\bar{r})\cdot E_{\text{inc}}(\bar{r}) \\ &+ \sum_{\substack{j=1\\ j\neq 1}}^{N}\sum_{\alpha=1}^{N_b} a_{j\alpha}\int_{V_l} d\bar{r}\bar{f}_{l\beta}(\bar{r})\cdot\bar{q}_{j\alpha}(\bar{r})\Bigg\}\end{aligned} \tag{183}$$

Equation (183) contains the full multiple scattering effects among the N number of spheroids under the small spheroid assumption. Because of the small spheroid assumption, only

the dipole term contributes to the first term in Eq. (183) which is the polarization induced by the incident field. Thus

$$\int_{V_l} d\overline{r}\overline{f}_{l\beta}(\overline{r}) \cdot \overline{E}_{\rm inc}(\overline{r}) = v_{0l}\overline{f}_{l\beta} \cdot \overline{E}_{\rm inc}(\overline{r}_l) \tag{184}$$

After the coefficients $a_{l\beta}$, $l = 1, 2, \ldots, N$, and $\beta = 1, 2, 3$ are solved, the far-field scattered field in the direction (θ_s, φ_s) is expressed as

$$\begin{aligned}\overline{E}_{\rm s}(\overline{r}) = k^2 \frac{e^{ikr}}{4\pi r}(\hat{\boldsymbol{v}}_{\rm s}\hat{\boldsymbol{v}}_{\rm s} + \hat{\boldsymbol{h}}_{\rm s}\hat{\boldsymbol{h}}_{\rm s}) \\ \cdot \sum_{j=1}^{N}\sum_{\alpha=1}^{N_b} a_{j\alpha}(\epsilon_{rj} - 1)\int_{V_j} d\overline{r}' e^{-i\overline{k}_{\rm s}\cdot\overline{r}'}\overline{f}_{j\alpha}(\overline{r}')\end{aligned} \tag{185}$$

where $\epsilon_{rj} = \epsilon_j/\epsilon$, $\hat{\boldsymbol{k}}_{\rm s} = \sin\theta_{\rm s}\cos\varphi_{\rm s}\hat{\boldsymbol{x}} + \sin\theta_{\rm s}\sin\varphi_{\rm s}\hat{\boldsymbol{y}} + \cos\theta_{\rm s}\hat{\boldsymbol{z}}$ is the scattered direction; $\hat{\boldsymbol{v}}_{\rm s} = \cos\theta_{\rm s}\cos\varphi_{\rm s}\hat{\boldsymbol{x}} + \cos\theta_{\rm s}\sin\varphi_{\rm s}\hat{\boldsymbol{y}} - \sin\theta_{\rm s}\hat{\boldsymbol{z}}$, $\hat{\boldsymbol{h}}_{\rm s} = -\sin\varphi_{\rm s}\hat{\boldsymbol{x}} + \cos\varphi_{\rm s}\hat{\boldsymbol{y}}$ are, respectively, the vertical and horizontal polarizations. Under the small spheroid assumption, only the dipole fields will contribute to the far-field radiation in Eq. (185). Thus, we have

$$\overline{E}_{\rm s}(\overline{r}) \cong k^2 \frac{e^{ikr}}{4\pi r}(\hat{\boldsymbol{v}}_{\rm s}\hat{\boldsymbol{v}}_{\rm s} + \hat{\boldsymbol{h}}_{\rm s}\hat{\boldsymbol{h}}_{\rm s}) \cdot \sum_{j=1}^{N}\sum_{\alpha=1}^{N_b} a_{j\alpha}(\epsilon_{rj} - 1)v_{0j}\overline{f}_{j\alpha}e^{-i\overline{k}_{\rm s}\cdot\overline{r}_j} \tag{186}$$

Numerical Simulation. In this section, we show the results of the numerical simulations by using $N = 2000$ spheroids and up to $f = 30\%$ by volume fraction. The relative permittivity used for the spheroids is 3.2 and the size parameter of the spheroids used is such that $ka = 0.2$. For dipole interactions, we replace the integral in the last term of Eq. (183) as follows.

$$\int_{V_l} d\overline{r}\overline{f}_{l\beta}(\overline{r}) \cdot \overline{q}_{j\alpha}(\overline{r}) = (\epsilon_{rj} - 1)v_{0j}v_{0l}k^2\overline{f}_{l\beta} \cdot \overline{\overline{G}}(\overline{r}_l, \overline{r}_j) \cdot \overline{f}_{j\alpha} \tag{187}$$

where

$$\overline{\overline{G}}(\overline{r}_l, \overline{r}_j) = \left(\overline{\overline{I}} + \frac{\overline{\nabla}\overline{\nabla}}{k^2}\right) g(\overline{r}, \overline{r}') \tag{188}$$

is the dyadic Green's function.

In the simulations, all the spheroids are prolate and are identical in size with $c = ea$, where e is the elongation ratio of the prolate spheroid. The size of the box in which the spheroids are placed is

$$V = Nv/f \tag{189}$$

where f is the fractional volume, and $v = 4\pi a^2 c/3$ is the volume of one spheroid. To create the situation of random phase, it is important that the size of the box has to be larger than a wavelength.

An incident electric field of

$$\overline{E}_{\rm inc}(\overline{r}) = \hat{y}e^{ikz} \tag{190}$$

is launched onto the box containing the N spheroids. The matrix of Eq. (183) is solved by iteration. After the matrix equation is solved, the scattered field is calculated by Eq. (186). The scattered field is decomposed into vertical and horizontal polarization

$$\overline{E}_{\rm s} = E_{vs}\hat{v}_{\rm s} + E_{hs}\hat{h}_{\rm s} \tag{191}$$

In the simulations of random discrete scatterer scattering, there is a strong component of coherent scattered field that is dependent on the shape of the box. To calculate the extinction rates and the scattering phase matrices, we need to subtract out the coherent field to get the incoherent fields. The incoherent fields contribute to the extinction rates and the scattering phase matrices. The simulations are performed for N_r realizations. We performed $N_r = 50$ realizations for this article. Let σ be the realization index. Then the coherent scattered field is

$$\langle E\rangle = \frac{r}{N_r}\sum_{\sigma=1}^{N_r}\overline{E}_{\rm s}^{\sigma} \tag{192}$$

and the incoherent field is

$$\overline{\epsilon}_{\rm s}^{\sigma} = r\overline{E}_{\rm s}^{\sigma} - \langle\overline{E}_{\rm s}\rangle \tag{193}$$

which also can be decomposed into vertical and horizontal polarization

$$\overline{\epsilon}_{\rm s}^{\sigma} = \epsilon_{vs}^{\sigma}\hat{v}_{\rm s} + \epsilon_{hs}^{\sigma}\hat{h}_{\rm s} \tag{194}$$

The averaged N particle bistatic scattering cross sections are

$$\sigma_{v_sN} = \frac{1}{N_r}\sum_{\sigma=1}^{N_r}|\epsilon_{vs}^{\sigma}|^2 \tag{195}$$

$$\sigma_{h_sN} = \frac{1}{N_r}\sum_{\sigma=1}^{N_r}|\epsilon_{hs}^{\sigma}|^2 \tag{196}$$

The N particle bistatic scattering cross sections of Eqs. (195) and (196) contain the collective scattering effects of the particles.

For the simulations, the particles are not absorptive. Thus the extinction rate is the same as the scattering rate. The extinction rate is

$$\kappa_{\rm e} = \frac{1}{V}\int_0^{\pi} d\theta_{\rm s}\sin\theta_{\rm s}\int_0^{2\pi} d\varphi_{\rm s}(\sigma_{\rm vsN} + \sigma_{\rm hsN}) \tag{197}$$

The $1/V$ factor in Eq. (197) is due to the fact that the extinction rate for a random medium is the extinction cross section per unit volume of space and the V in this case is the size of the box. The random positions of the spheroids are generated by a shuffling method facilitated by contact function (20,21).

In Fig. 11, we illustrate the extinction coefficients normalized by the wavenumber k as a function of fractional volume. We consider the case consisting of aligned prolate spheroids with $ka = 0.2$ and $e = 1.8$. In such a medium, a vertically polarized incident wave with the incident polarization aligned with the symmetry axis of the prolate spheroids has a higher extinction rate than that of the horizontally polarized incident wave. The extinction rate is polarization dependent. In the same figure, we also show the extinction rate for the case when the spheroids are randomly oriented. For random orien-

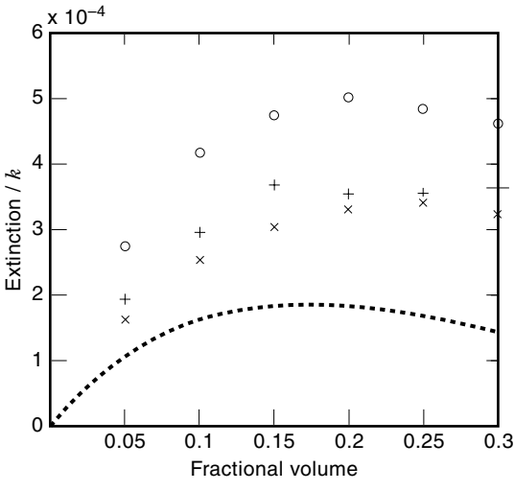

Figure 11. Extinction rate as a function of fractional volume of particles. Relative permittivity of particles $\epsilon_r = 3.2$. For spheroids $ka = 0.2$ and $e = 1.8$. For spheres $ka = 0.2$. The dotted curve is for the medium with spheres; +, the medium with randomly oriented spheroids. o and x, the medium with aligned spheroids but with incident wave being vertically and horizontally polarized, respectively.

tation, the probability density function of orientation $p(\beta, \alpha)$ is

$$p(\beta, \alpha) = \frac{\sin\beta}{4\pi}$$

for $0 \le \beta \le \pi$, and $0 \le \alpha \le 2\pi$. The $\sin\beta$ is a result of the smaller solid angle at small β. The normalization of the probability density function is such that

$$\int_0^{2\pi} d\alpha \int_0^{\pi} d\beta p(\beta, \alpha) = 1$$

The attenuation for the randomly oriented case is between those of vertically and horizontally polarized incidence of the aligned case. The extinction rates are also compared with those of a medium with spherical particles of $ka = 0.2$ and $e = 1$. The spherical case predicts a much lower attenuation than the spheroidal case, even though the medium has the same fractional volume.

Next we illustrate the scattering phase matrices. The phase matrices are bistatic scattering cross sections per unit volume of a conglomeration of particles. We consider the incident wave and polarization as given by Eq. (190). The spheroids are randomly oriented in the following illustrations. We also compare with the results of independent scattering. The independent scattering results are obtained by including only the first term inside the curly bracket of Eq. (183). That is,

$$a_{l\beta} = \frac{1}{(1 - C_{l\beta})} \int_{V_l} d\bar{r} \bar{f}_{l\beta}(\bar{r}) \cdot \bar{E}_{\text{inc}}(\bar{r}) \tag{198}$$

CASE 1. $\varphi_s = 0°$ and $\varphi_s = 180°$. For this case, we define the phase matrix elements of

$$P_{11}(\theta_s) = \frac{\sigma_{vsN}}{V} \tag{199}$$

$$P_{21}(\theta_s) = \frac{\sigma_{hsN}}{V} \tag{200}$$

In this case, the incident polarization is perpendicular to the scattering plane formed by the incident and scattered directions. The quantities P_{11} and P_{21} correspond to copolarization and cross-polarization, respectively. In Figs. 12(a) and 12(b), we plot P_{11} and P_{21}, respectively, as a function of θ_s. We give the results of $\varphi_s = 0°$ and $\varphi_s = 180°$ in the same figure. The following definition is used. For $\varphi_s = 0°$, we have a scattering angle between 0° and 180° and the scattering angle is equal to θ_s. For $\varphi_s = 180°$, the scattering angle is equal to $360° - \theta_s$ covering the range of scattering angles between 180° and 360°.

CASE 2. $\varphi_s = 90°$ and $\varphi_s = 270°$. For this case, we define the phase matrix elements of

$$P_{12}(\theta_s) = \frac{\sigma_{\text{hsN}}}{V} \tag{201}$$

$$P_{22}(\theta_s) = \frac{\sigma_{\text{vsN}}}{V} \tag{202}$$

In this case, the incident polarization is in the scattering plane formed by the incident and scattered directions. The quantities P_{22} and P_{12} correspond to copolarization and cross polarization, respectively. In Figs. (12c) and Figs. (12d), we plot P_{12} and P_{22}, respectively, as a function of θ_s. The scattering angle is between 0° and 360°. The following definition is used. For $\varphi_s = 90°$, we have the scattering angle between 0° and 180° the scattering angle is equal to θ_s. For $\varphi_s = 270°$, the scattering angle is equal to $360° - \theta_s$ covering the range of scattering angles between 180° and 360°. In Fig. 12, we show the results of P_{11}, P_{21}, P_{12}, and P_{22} for the fractional volume of 30%. The results of independent scattering are also shown for comparison. The dimension of phase matrix is bistatic cross section per unit volume which is inverse distance. The unit is such that wavelength is equal to unity. We note that the copolarization, P_{11} and P_{22}, are smaller than those of independent scattering, whereas the cross-polarization, P_{21} and P_{12}, are higher than those of independent scattering. We also note that the simulation results fluctuate because of the random phase situation, whereas that of independent scattering are smooth curves. The fluctuations are characteristic of random scattering as the bistatic scattering cross section per unit volume will fluctuate from sample to sample. We also note that P_{22} has angular dependence that is the characteristic of Rayleigh scattering.

Simulations of Scattering by Random Rough Surface

The classical analytic approaches of solving random rough surface scattering problems based on the Kirchhoff approximation and small perturbation method are restricted in domain of validity (1,2). Recently, there has been an increasing interest in the Monte-Carlo simulations of random rough surface scattering. One method is the integral equation method in which an integral equation is then converted to a matrix

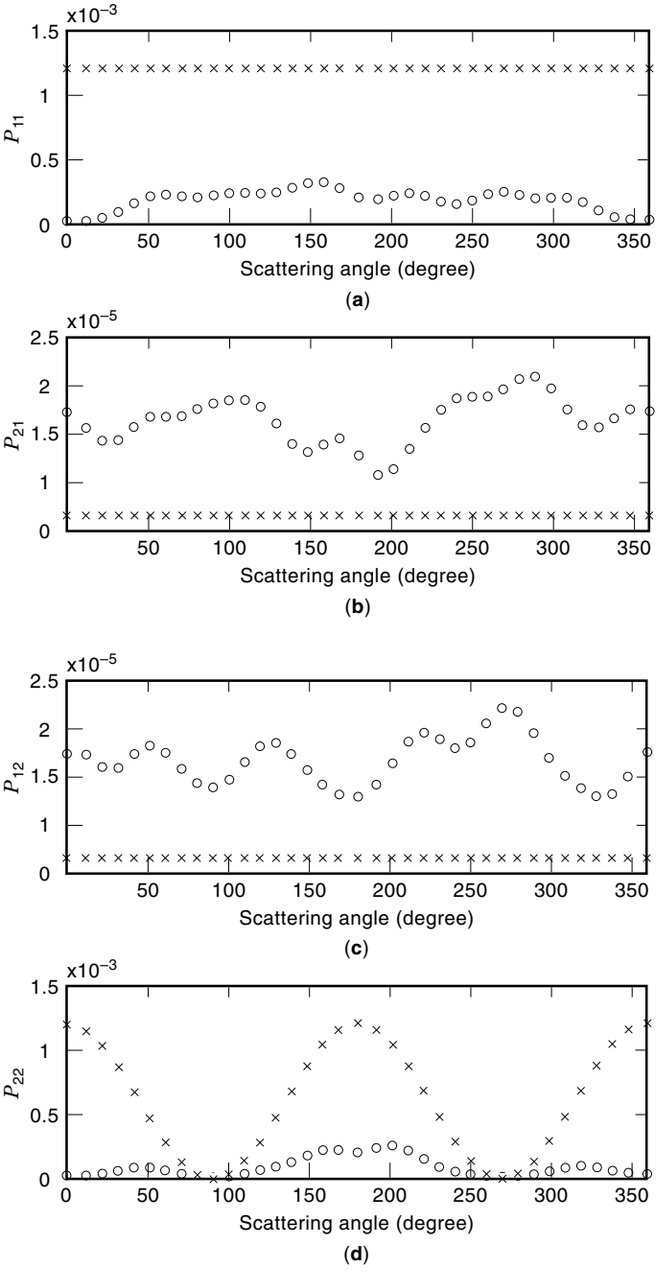

Figure 12. Phase matrix as a function of scattering angle for $ka = 0.2$, fractional volume $f = 30\%$, elongation ratio $e = 1.8$, relative permittivity of particles $\epsilon_r = 3.2$. The spheroids are randomly oriented. In the simulations, $N = 2000$ particles are used and the results are averaged over $N_r = 50$ realizations. (a) P_{11}, (b) P_{21}, (c) P_{21}, and (d) P_{22}. o, the dense medium results. x, the independent scattering results.

equation by the method of moments, and the resulting equation is solved with a full matrix inversion. Many practical problems such as the near-grazing incidence or two-dimensional rough surface are considered large-scale rough surface problems. For such large-scale rough surface problems, an efficient numerical method is needed. The simulation of large-scale rough surface problem have been a subject of intensive research in recent years (22,23). Fast numerical methods have been developed to solve such problems (24–28). In this section, we shall use a standard method of simulation and illustrate the results. The numerical results yield many interesting features that are beyond the validity of classical methods.

Integral Equation. We confine our attention to numerical simulations of scattering by one-dimensional random rough surface. Consider an incident wave $\psi_{\text{inc}}(\bar{r})$ impinging upon a one-dimensional random rough surface with a height profile $z = f(x)$. The wave function $\psi(\bar{r})$ above the surface is

$$\psi(\bar{r}) = \psi_{\text{inc}}(\bar{r}) + \psi_s(\bar{r}) \tag{203}$$

where $\psi_s(\bar{r})$ is the scattered wave. The wave function obeys the following surface integral equation

$$\psi_{\text{inc}}(\bar{r}') + \int_S ds\hat{\boldsymbol{n}} \cdot [\psi(\bar{r})\overline{\nabla} g(\bar{r}, \bar{r}') - g(\bar{r}, \bar{r}')\overline{\nabla}\psi(\bar{r})]$$

$$= \begin{cases} \psi(\bar{r}') & \bar{r}' \in V_0 \quad (204a) \\ \dfrac{1}{2}\psi(\bar{r}') & \bar{r}' \in S \quad (204b) \\ 0 & \bar{r}' \in V_1 \quad (204c) \end{cases}$$

where

$$g(\bar{r}, \bar{r}') = \frac{i}{4} H_0^{(1)}(k|\bar{r} - \bar{r}'|) \tag{205}$$

is the two-dimensional Green's function. The zero in Eq. (204c) corresponds to the extinction theorem. Note that in Eqs. (204a) and (204b), $\bar{r}$ is on the surface.

The transmitted wave $\psi_1(\bar{r})$ in the lower medium satisfies

$$\int_S ds\hat{\boldsymbol{n}} \cdot [\psi_1(\bar{r})\overline{\nabla} g_1(\bar{r}, \bar{r}') - g_1(\bar{r}, \bar{r}')\overline{\nabla}\psi_1(\bar{r})]$$

$$= \begin{cases} 0 & \bar{r}' \in V_0 \quad (206a) \\ -\dfrac{1}{2}\psi_1(\bar{r}') & \bar{r}' \in S \quad (206b) \\ -\psi_1(\bar{r}') & \bar{r}' \in V_1 \quad (206c) \end{cases}$$

where

$$g_1(\bar{r}, \bar{r}') = \frac{i}{4} H_0^{(1)}(k_1|\bar{r} - \bar{r}'|) \tag{207}$$

is Green's function of the lower medium.

The wave functions $\psi(\bar{r})$ and $\psi_1(\bar{r})$ are related by boundary condition on surface S. For the TE wave, the boundary condition is

$$\psi(\bar{r}) = \psi_1(\bar{r}) \tag{208a}$$

$$\hat{\boldsymbol{n}} \cdot \overline{\nabla}\psi(\bar{r}) = \hat{\boldsymbol{n}} \cdot \overline{\nabla}\psi_1(\bar{r}) \tag{208b}$$

For the TM wave, the boundary condition is

$$\psi(\bar{r}) = \psi_1(\bar{r}) \tag{209a}$$

$$\frac{1}{\epsilon}\hat{\boldsymbol{n}} \cdot \overline{\nabla}\psi(\bar{r}) = \frac{1}{\epsilon_1}\hat{\boldsymbol{n}} \cdot \overline{\nabla}\psi_1(\bar{r}) \tag{209b}$$

By rewriting Eq. (204b) and applying the boundary condition to Eq. (206b), we have

$$\psi_{\text{inc}}(\bar{r}') + \int_S ds[\psi(\bar{r})\hat{\boldsymbol{n}} \cdot \overline{\nabla} g(\bar{r}, \bar{r}') - g(\bar{r}, \bar{r}')\hat{\boldsymbol{n}} \cdot \overline{\nabla}\psi(\bar{r})] = \frac{1}{2}\psi(\bar{r}') \tag{210a}$$

$$\int_S ds[\psi(\bar{r})\hat{\boldsymbol{n}} \cdot \overline{\nabla} g_1(\bar{r}, \bar{r}') - g_1(\bar{r}, \bar{r}')\rho\hat{\boldsymbol{n}} \cdot \overline{\nabla}\psi(\bar{r})] = -\frac{1}{2}\psi(\bar{r}') \tag{210b}$$

where

$$\rho = \begin{cases} 1 & \text{for the TE wave} \\ \dfrac{\epsilon_1}{\epsilon} & \text{for the TM wave} \end{cases} \tag{211}$$

and $ds = [1 + (df/dx)^2]^{1/2}\, dx$. Let

$$u(\bar{r}, \bar{r}') = \sqrt{1 + (df/dx)^2}\hat{\boldsymbol{n}} \cdot \overline{\nabla}\Psi(\bar{r}, \bar{r}')$$

where $\bar{r} = \bar{r}[x, f(x)]$ and $\bar{r}' = \bar{r}'[x', f(x')]$. Using the method of moment (18), we can discretize the above equations as

$$\sum_{n=1}^{N} a_{mn} u(x_n) + \sum_{n=1}^{N} b_{mn}\psi(x_n) = \psi_{\text{inc}}(x_m) \tag{212a}$$

$$\sum_{n=1}^{N} a_{mn}^{(1)} \rho u(x_n) + \sum_{n=1}^{N} b_{mn}^{(1)}\psi(x_n) = 0 \tag{212b}$$

where $x_m = (m - 0.5)\Delta x - L/2$, $m = 1, 2, \ldots, N$. The matrix elements a_{mn}, b_{mn}, $a_{mn}^{(1)}$, and $b_{mn}^{(1)}$ are given by

$$a_{mn} = \begin{cases} \Delta x \dfrac{i}{4} H_0^{(1)}(kr_{mn}) & m \neq n \\ \Delta x \dfrac{i}{4} H_0^{(1)}[k\Delta x\gamma_m/(2e)] & m = n \end{cases} \tag{213}$$

$$b_{mn} = \begin{cases} -\Delta x \dfrac{ik}{4} \dfrac{f'(x_n)(x_n - x_m) - [f(x_n) - f(x_m)]}{r_{mn}} H_1^{(1)}(kr_{mn}) & m \neq n \\ \dfrac{1}{2} - \dfrac{f''(x_m)}{4\pi} \dfrac{\Delta x}{\gamma_m^2} & m = n \end{cases} \tag{214}$$

$$a_{mn}^{(1)} = \begin{cases} \Delta x \dfrac{i}{4} H_0^{(1)}(k_1 r_{mn}) & m \neq n \\ \Delta x \dfrac{i}{4} H_0^{(1)}[k_1\Delta x\gamma_m/(2e)] & m = n \end{cases} \tag{215}$$

$$b_{mn}^{(1)} = \begin{cases} -\Delta x \dfrac{ik_1}{4} \dfrac{f'(x_n)(x_n - x_m) - [f(x_n) - f(x_m)]}{r_{mn}} H_1^{(1)}(k_1 r_{mn}) & m \neq n \\ -\dfrac{1}{2} - \dfrac{f''(x_m)}{4\pi} \dfrac{\Delta x}{\gamma_m^2} & m = n \end{cases} \tag{216}$$

where $r_{mn} = \{(x_n - x_m)^2 + [f(x_n) - f(x_m)]^2\}^{1/2}$ and $\gamma_m = \{1 + [f'(x_m)]^2\}^{1/2}$, $e = 2.71828183$, $H_1^{(1)}$ is the first-order Hankel function of the first kind, and $f'(x_m)$ and $f''(x_m)$ represent the first and second derivative of $f(x)$ evaluated at x_m, respectively.

Incident Waves and Scattered Waves. In numerical simulations, the rough surface is truncated at $x = \pm L/2$. This means that the surface current is truncated at $x = \pm L/2$, so that the surface current is forced to zero for $|x| > L/2$. If this is an abrupt change, artificial reflection from the two endpoints will occur. To avoid these artificial reflections, one common way is to taper the incident wave so that the incident wave decays to zero gradually and are exponentially small outside the domain. A way to taper the incident wave is in the spectral domain. Let

$$\psi_{\text{inc}}[x, f(x)] = \frac{g}{2\sqrt{\pi}} \int_{-\infty}^{\infty} dk_x e^{i(k_x x - k_z z)} e^{-\frac{(k_x - k_{ix})^2 g^2}{4}} \tag{217}$$

where $k_{ix} = k \sin\theta_i$, $k_z^2 = k^2 - k_x^2$, k is the wavenumber of the free space, and g is the parameter that controls the tapering of the incident wave. The advantage of using Eq. (217) is that it obeys the wave equation exactly because it is a spectrum of plane waves.

To calculate the power impinging upon the surface, we have

$$\overline{S}_{\text{inc}} \cdot \hat{z} = -\frac{1}{2\eta k} \text{Im}\left(\psi_{\text{inc}} \frac{\partial \psi_{\text{inc}}^*}{\partial z}\right) \tag{218}$$

The power received is

$$P_{\text{inc}} = -\int_{-\infty}^{\infty} dx \overline{S}_{\text{inc}} \cdot \hat{\boldsymbol{z}} \tag{219}$$

By substituting Eq. (218) into (219) and integrating over dx, it follows readily that only propagating waves contribute to power. Thus

$$P_{\text{inc}} = \frac{g^2}{4\eta k} \int_{-k}^{k} dk_x k_z \exp\left[-\frac{(k_x - k_{ix})^2 g^2}{4}\right] \tag{220}$$

Scattered Waves. After the surface fields $\psi(\bar{r})$ and $\boldsymbol{n} \cdot \overline{\nabla}\psi(\bar{r})$ are calculated by numerical methods, we can calculate the scattered waves and the transmitted waves using Eqs. (204a) and (206c), respectively. From Eq. (204a), the scattered wave is

$$\psi_{\text{s}}(\bar{r}') = \int_S ds[\psi(\bar{r})\hat{\boldsymbol{n}} \cdot \overline{\nabla} g(\bar{r}, \bar{r}') - g(\bar{r}, \bar{r}')\hat{\boldsymbol{n}} \cdot \overline{\nabla}\psi(\bar{r})] \tag{221}$$

For the far field

$$g(\bar{r}, \bar{r}') = \frac{i}{4}\sqrt{\frac{2}{\pi k r'}} \exp\left(-i\frac{\pi}{4}\right) \exp(ikr') \exp[-ik(\sin\theta_s x + \cos\theta_s z)] \tag{222}$$

Putting Eq. (222) and into (221), we have

$$\psi_{\text{s}}(\bar{r}') = \frac{i}{4}\sqrt{\frac{2}{\pi k r'}} \exp\left(-i\frac{\pi}{4}\right) \exp(ikr')\psi_s^{(N)}(\theta_s) \tag{223}$$

where

$$\psi_{\text{s}}^{(N)}(\theta_{\text{s}}) = \int_{-\infty}^{\infty} dx \left\{-u(x) + \psi(x)ik\left[\frac{df}{dx}\sin\theta_{\text{s}} - \cos\theta_{\text{s}}\right]\right\} \exp[-ik(x \sin\theta_{\text{s}} + f(x)\cos\theta_{\text{s}})] \tag{224}$$

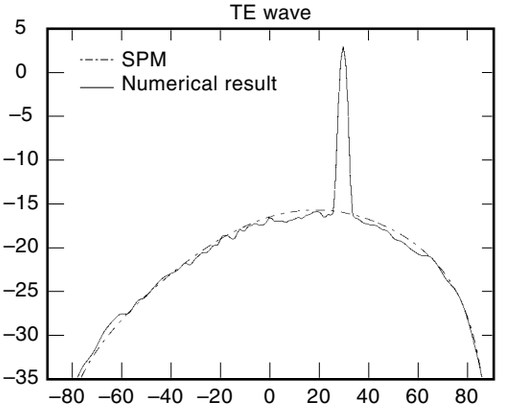

Figure 13. Numerical results of wave scattering from a dielectric slightly rough surface and comparison with the small perturbation method (SPM) for the case of rms height of 0.05 wavelength, correlation length of 0.35 wavelength and relative dielectric constant of 5.6 + i0.6 at an incidence angle of 30°. The numerical results are averaged over 200 realizations. The results show good agreement between the numerical method and SPM for the case of small rms height for TE wave incidence.

The Poynting's vector in direction $\hat{\boldsymbol{k}}_s$ is

$$\overline{S}_s(\overline{r}') = -\frac{1}{2\eta k}\mathrm{Im}[\psi_s(r)\overline{\nabla}\psi_s^*(r')] \tag{225}$$

The total power scattered above the surface is

$$\begin{aligned} P_s &= \int_{-\pi/2}^{\pi/2} d\theta_s r S_s(\overline{r}') \\ &= \int_{-\pi/2}^{\pi/2} \frac{1}{2\eta}\frac{1}{16}\frac{2}{\pi k}|\psi_s^{(N)}(\theta_s)|^2 \end{aligned} \tag{226}$$

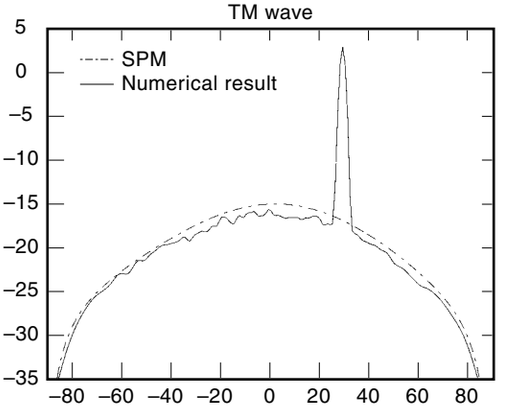

Figure 14. Numerical results of wave scattering from a dielectric slightly rough surface and comparison with the small perturbation method (SPM) for the case of rms height of 0.05 wavelength, correlation length of 0.35 wavelength and relative dielectric constant of 5.6 + i0.6 at incidence angle of 30°. The numerical results are averaged over 200 realizations. The results show good agreement between the numerical method and SPM for the case of small rms height for TM wave incidence.

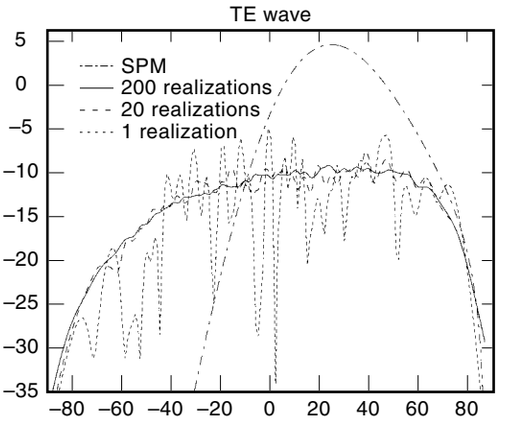

Figure 15. The convergence test with respect to number of realizations for the TE case and comparison with the small perturbation method for the case of rms height of 0.3 wavelength, correlation length of 1 wavelength and relative dielectric constant of 5.6 + i0.6 at the incidence angle of 30°. The numerical results show that we need many realizations for the convergence of the averaged bistatic scattering coefficients. Also SPM cannot give accurate results for the moderate rms height.

To define the bistatic scattering coefficient $\sigma(\theta_s)$, we have

$$\frac{P_s}{P_{inc}} = \int_{-\pi/2}^{\pi/2} d\theta_s \sigma(\theta_s) \tag{227}$$

Thus

$$\sigma(\theta_s, \theta_i) = \frac{|\psi_s^{(N)}(\theta_s)|^2}{4\pi g^2 \int_{-k}^{k} dk_x k_z \exp[-(k_x - k\sin\theta_i)^2 g^2/2]} \tag{228}$$

Results of Numerical Simulations. In this section, results of numerical simulations are illustrated. First, we show the bistatic scattering coefficient of a rough surface with small rms height and slope and compare them with that from the small perturbation method. Next, we illustrate the convergence with respect to the number of realizations. After that, wave

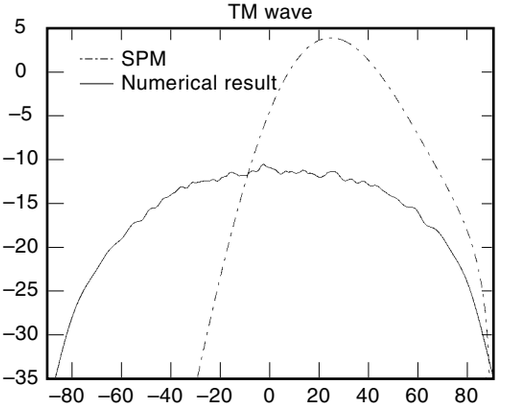

Figure 16. Numerical results of wave scattering from the dielectric rough surface with a moderate rms height and comparison with the small perturbation method. TM case.

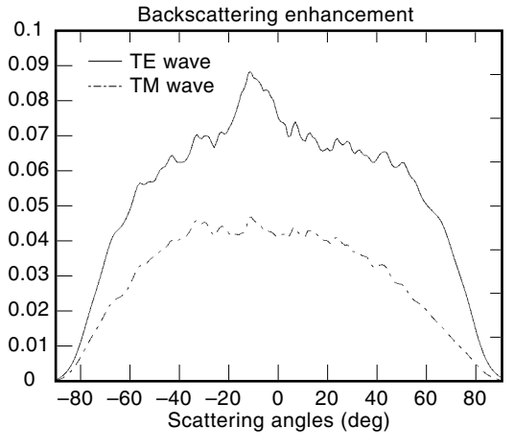

Figure 17. Numerical results of wave scattering from a dielectric rough surface with a large rms height. Backscattering enhancement is shown for both TE and TM waves. This result indicates the importance of multiple scattering effects.

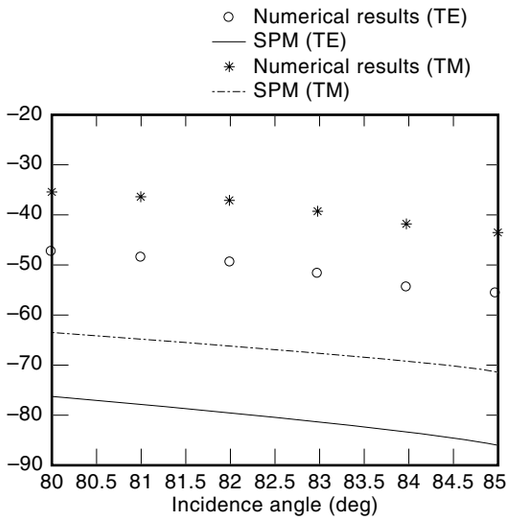

Figure 19. The variation of backscattering coefficients as a function of incidence angles from 80° and 85° and comparison with the small perturbation method.

scattering from a very rough surface is calculated so that backscattering enhancement (27) can be observed. The variations of emissivities with incidence angles and permittivities are plotted too. Finally, backscattering coefficients at low grazing angle are shown.

In Figs. 13 and 14, we plot the numerical results averaged over 200 realizations for TE and TM waves, respectively, for the case of rms $h = 0.05\lambda$, correlation length 0.35λ, incident angle 30°, and $5.6 + i0.6$ of relative dielectric constant. We also show the results of using the small perturbation method (SPM). We see that the two results are in very good agreement. Because of the small height, we see a distinct angular peak in the specular direction of $\theta_s = \theta_i = 30°$. The peak is due to specular reflection of the coherent wave. Because of its small slope, $\sigma(\theta_s)$ decreases rapidly away from the specular direction. In Fig. 15, we test the convergence with respect to the number of realizations for the TE case. We show the results averaged over 1, 20, and 200 realizations, respectively.

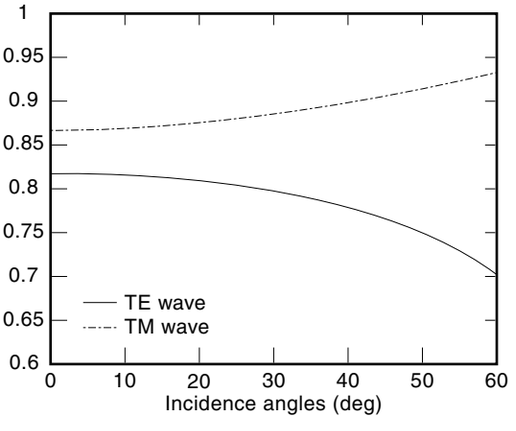

Figure 18. The variation of emissivities with the incident angles.

The rms height of rough surface is 0.3λ, correlation length is 1.0λ, the relative dielectric constant of lower medium is $5.6 + i0.6$, and the incident angle is 30°. For one realization, there are angular fluctuations of the bistatic scattering coefficients, which is a result of constructive and destructive interferences as a function of θ_s. With the increasing of the number of realizations, the curve becomes smoother and smoother. SPM results are also shown in the figure. In this case, because of larger rms height, the two results are different. That means we can not use SPM for larger rms height. In Fig. 16, we plot the results with the same parameters as in Fig. 15 for the TM case. The results indicate that there are large differences between numerical simulation and SPM. In Fig. 17, the bistatic scattering coefficients are shown for the case with large rms height and slope for both TE and TM waves. The case is with rms $h = 0.5\lambda$, correlation length 1.0λ, and relative dielectric constant $5.6 + i0.6$ at incidence angle of 10°. The backscattering enhancement is observed for both TE and TM waves. In passive remote sensing, the emissivity is an important parameter. It relates the brightness temperatures to the physical temperature.

The emissivity can be calculated by integrating bistatic scattering coefficients over scattering angles and subtracting the result from unity. In Fig. 18, the variation of emissivities with the incident angles are illustrated for the case of rms $h = 0.3\lambda$, correlation length 1.0λ, and dielectric constant $5.6 + i0.6$ for TE and TM cases, repectively. We can see that the emissivity of the TE wave decreases as the incidence angle increases. For the TM wave, the emissivity increases as the incidence angle increases. In Fig. 19, we study the case of close-to-grazing incidence by plotting the TE and TM backscattering coefficients as a function of incidence angles from 80° and 85°. The results of the SPM are also shown. Both TE and TM backscattering coefficients decreases as a function of incidence angle. There are large differences between numerical simulations and the SPM.

BIBLIOGRAPHY

1. A. Ishimaru, *Wave Propagation and Scattering in Random Media,* Vols. 1 and 2, New York: Academic Press, 1978.
2. L. Tsang, J. A. Kong, and R. T. Shin, *Theory of Microwave Remote Sensing,* New York: Wiley-Interscience, 1985.
3. A. G. Voronovich, *Wave Scattering from Rough Surfaces,* New York: Springer-Verlag, 1994.
4. F. T. Ulaby, R. K. Moore, and A. K. Fung, *Microwave Remote Sensing: Active and Passive,* Vols. 1 and 2, Reading, MA: Addison-Wesley, 1981.
5. F. T. Ulaby and C. Elachi, *Radar Polarimetry for Geoscience Applications,* Norwood, MA: Artech House, 1990.
6. P. Sheng (ed.), *Scattering and Localization of Classical Waves in Random Media,* Singapore: World Scientific, 1990.
7. S. Chandrasekhar, *Radiative Transfer,* New York: Dover, 1960.
8. L. Landau and E. Lifshitz, *Electrodynamics of Continuous Media,* Oxford, UK: Pergamon, 1960.
9. S. O. Rice, Reflection of EM waves by slightly rough surface, in M. Kline (ed.), *The Theory of Electromagnetic Waves,* New York: Interscience, 1963.
10. L. L. Foldy, The multiple-scattering of waves, *Phys. Rev.,* **67**: 107–119, 1945.
11. L. Tsang, Thermal emission of nonspherical particles, *Radio Sci.,* **19**: 966–974, 1984.
12. A. K. Fung, *Microwave Scattering and Emission Models and their Applications,* Boston: Artech House, 1994.
13. R. F. Millar, The Rayleigh hypothesis and a related least squares solution to scattering problems for periodic surfaces and other scatterers, *Radio Sci.,* **8**: 785–796, 1973.
14. A. A. Maradudin, R. E. Luna, and E. R. Mendez, The Brewster effect for a one-dimensional random surface, *Waves Random Media,* **3** (1): 51–60, 1993.
15. J. J. Greffet, Theoretical model of the shift of the Brewster angle on a rough surface, *Opt. Lett.,* **17**: 238–240, 1992.
16. A. Ishimaru and Y. Kuga, Attenuation constant of coherent field in a dense distribution of particles, *J. Opt. Soc. Am.,* **72**: 1317–1320, 1982.
17. K. H. Ding et al., Monte Carlo simulations of pair distribution functions of dense discrete random media with multiple sizes of particles, *J. Electro. Waves Appl.,* **6**: 1015–1030, 1992.
18. R. F. Harrington, *Field Computation by Moment Methods,* New York: MacMillan, 1968.
19. J. Stratton, *Electromagnetic Theory,* New York: McGraw-Hill, 1941.
20. J. W. Perram et al., Monte Carlo simulations of hard spheroids, *Chem. Phys. Lett.,* **105**: 277–280, 1984.
21. J. W. Perram and M. S. Wertheim, Statistical mechanics of hard ellipsoids. I. Overlap algorithm and the contact function, *J. Comp. Phys.,* **58**: 409–416, 1985.
22. E. Thorsos and D. Jackson, Studies of scattering theory using numerical methods, *Waves Random Media,* **1** (3): 165–190, 1991.
23. M. Nieto-Vesperinas and J. M. Soto-Crespo, Monte-Carlo simulations for scattering of electromagnetic waves from perfectly conducting random rough surfaces, *Opt. Lett.,* **12**: 979–981, 1987.
24. L. Tsang et al., Monte Carlo simulations of large-scale problems of random rough surface scattering and applications to grazing incidence with the BMIA/canonical grid method, *IEEE Trans. Antennas Propag.,* **AP-43**: 851–859, 1995.
25. K. Pak et al., Backscattering enhancement of vector electromagnetic waves from two-dimensional perfectly conducting random rough surfaces based on Monte Carlo simulations, *J. Opt. Soc. Amer. A,* **12** (11): 2491–2499, 1995.
26. K. Pak, L. Tsang, and J. T. Johnson, Numerical simulations and backscattering enhancement of electromagnetic waves from two-dimensional dielectric random rough surfaces with the sparse-matrix canonical method, *J. Opt. Soc. Amer. A,* **14** (7): 1515–1529, 1997.
27. J. T. Johnson et al., Backscattering enhancement of electromagetic waves from two-dimensional perfectly conducting random rough surfaces: A comparison of Monte Carlo simulations with experimental data, *IEEE Trans. Antennas Propag.,* **AP-44**: 748–756, 1996.
28. V. Jandhyala et al., A combined steepest descent-fast multiple algorithm for the fast analysis of three-dimensional scattering by rough surface, *IEEE Trans. Geosci. Remote Sens.,* **36**: 738–748, 1998.
29. L. Tsang, Polarimetric passive microwave remote sensing of random discrete scatterers and rough surfaces, *J. Electro. Waves and Appli.,* **5** (1): 41–57, 1991.
30. S. H. Yueh et al., Polarimetric measurements of sea surface brightness temperature using an aircraft K-band Radiometer, *IEEE Trans. Geosci. Remote Sensing,* **33** (1): 85–92, Jan. 1995.

LEUNG TSANG
QIN LI
University of Washington

MICROWAVE RESONATORS. See CAVITY RESONATORS.